

Access to this work was provided by the University of Maryland, Baltimore County (UMBC) ScholarWorks@UMBC digital repository on the Maryland Shared Open Access (MD-SOAR) platform.

Please provide feedback

Please support the ScholarWorks@UMBC repository by emailing [scholarworks-group@umbc.edu](mailto:scholarworks-group@umbc.edu) and telling us what having access to this work means to you and why it's important to you. Thank you.

# **TRPM5-expressing Microvillous Cells Regulate Region-specific Cell Proliferation and Apoptosis during Chemical Exposure**

Kayla Lemons<sup>1</sup>, Ziying Fu<sup>1</sup>, Tatsuya Ogura<sup>1</sup> and Weihong Lin<sup>1</sup>

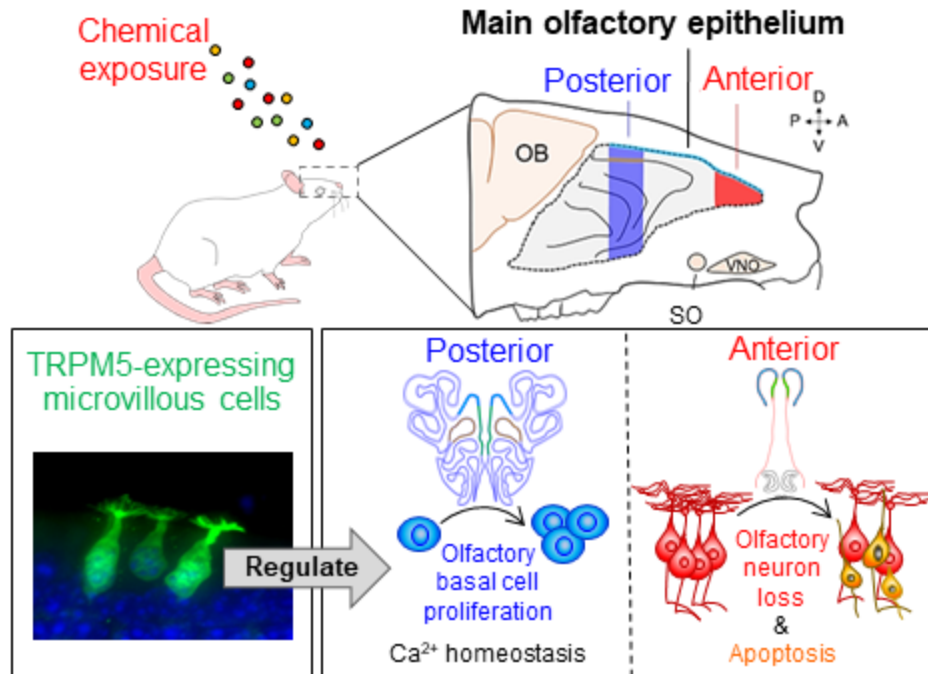
<sup>1</sup> Department of Biological Sciences, University of Maryland Baltimore County, Baltimore, MD 21250, USA

Abbreviated title: TRPM5-MC-dependent olfactory adaptive plasticity

Corresponding Author: Dr. Weihong Lin, Dept. of Biological Sciences, University of Maryland Baltimore County, 1000 Hilltop Circle, Baltimore, MD 21250 (e-mail: [weihong@umbc.edu](mailto:weihong@umbc.edu))

Number of figures and tables (separately): 8 and 1

Declarations of interest: none



## Research highlights

- Cholinergic TRPM5-expressing microvillous cells (TRPM5-MCs) are present throughout the main olfactory epithelium.
- We identify a novel role of TRPM5-MCs in modulating cell proliferation and tissue remodeling during chemical exposure.
- The data shed light on olfactory maintenance and the protective function of TRPM5-MCs in challenging chemical environments.

## Abstract

The mammalian main olfactory epithelium (MOE) is exposed to a wide spectrum of external chemicals during respiration and relies on adaptive plasticity to maintain its structural and functional integrity. We previously reported that the chemo-responsive and cholinergic transient receptor potential channel M5 (TRPM5)-expressing-microvillous cells (MCs) in the MOE are required for maintaining odor-evoked electrophysiological responses and olfactory-guided behavior during two-week exposure to an inhaled chemical mixture. Here, we investigated the underlying factors by assessing the potential modulatory effects of TRPM5-MCs on MOE morphology and cell proliferation and apoptosis, which are important for MOE maintenance. In the posterior MOE of TRPM5-GFP mice, we found that two-week chemical-exposure induced a significant increase in Ki67-expressing proliferating basal stem cells without a significant

reduction in the thickness of the whole epithelium or mature olfactory sensory neuron (OSN) layer. This adaptive increase in stem cell proliferation was missing in chemical-exposed transcription factor *Skn-1a* knockout (*Skn-1a*<sup>-/-</sup>) mice lacking TRPM5-MCs. In addition, a greater number of isolated OSNs from chemical exposed *Skn-1a*<sup>-/-</sup> mice displayed unhealthily high levels of resting intracellular Ca<sup>2+</sup>. Intriguingly, in the anterior MOE where we found a higher density of TRPM5-MCs, chemical-exposed TRPM5-GFP mice exhibited a time-dependent increase in apoptosis and a loss of mature OSNs without a significant increase in proliferation or neurogenesis to compensate for OSN loss. Together, our data suggest that TRPM5-MC-dependent region-specific upregulation of cell proliferation in the majority of the MOE during chemical exposure contributes to the adaptive maintenance of OSNs and olfactory function.

### **Keywords**

olfactory epithelium, inhalation exposure, intracellular calcium, adaptive plasticity, apoptosis, proliferation

### **Introduction**

Adaptive plasticity ensures that a sensory organ's optimal function is maintained in a changing environment. In terrestrial vertebrates, the main olfactory epithelium (MOE) is located in the nose, or the entrance of the respiratory tract, where it detects airborne molecules and monitors inhaled air quality to protect the lower airway and lungs. This anatomical arrangement, however, exposes the MOE to various degrees of chemical insults. In order to maintain MOE structure and function, multipotent stem cells in the basal layer of the MOE generate newborn cells to replace those that are aged or damaged, especially olfactory sensory neurons (OSNs) that detect airborne odor molecules throughout the lifetime (Graziadei & Graziadei, 1979; Calof et al., 1996; Huard et al., 1998; for review see Schwob et al., 2017). However, factors and pathways connecting harmful chemical detection to active cell proliferation and apoptosis are poorly understood.

The microvillous cells (MCs) in the MOE can be divided into distinct subpopulations based on their morphology, cell marker expression and functions (Moran et al., 1982; Carr et al., 1991; Elsaesser et al., 2005; Hansen & Finger 2008; Lin et al., 2007, 2008; Hegg et al., 2010; Ogura et al., 2011; Pfister et al., 2012, 2015; Jia et al., 2013; Lemons et al., 2017; Fu et al., 2018; Genovese & Tizzano, 2018). Following our initial identification and characterization of transient receptor potential melastatin 5 (TRPM5)-expressing non-neuronal MCs (Lin et al., 2007, 2008), we showed that TRPM5-MCs respond to relatively high concentrations of odorants

by increasing intracellular  $\text{Ca}^{2+}$ , leading to vesicle release and recycling (Fu et al., 2018). Also, TRPM5-MCs are capable of synthesizing and releasing acetylcholine (ACh), which differentially modulates intracellular  $\text{Ca}^{2+}$  in OSNs and supporting cells (SCs) via different muscarinic ACh receptors (Ogura et al., 2011; Fu et al., 2018). Furthermore, transcription factor *Skn-1a* knockout mice (*Skn-1a*<sup>-/-</sup>; Matsumoto et al., 2011) lacking TRPM5-MCs (Yamaguchi et al., 2014) exhibited impaired odor-evoked electroolfactogram (EOG) responses and olfactory-guided behavior after two-week exposure to inhaled relatively mild irritating chemicals (Lemons et al., 2017). These results suggest that TRPM5-MCs are the essential component of the newly identified intrinsic cholinergic network which adaptively modulates MOE activity to maintain olfactory function in challenging chemical environments (Ogura et al., 2011; Lemons et al., 2017; Fu et al., 2018).

Whether the cholinergic network activity influences cell turnover to maintain optimal MOE function is not known. ACh potentially increases intracellular  $\text{Ca}^{2+}$  levels (Ogura et al., 2011) and potentiates endocytosis in SCs via muscarinic M3 receptors (Fu et al., 2018). Thus, TRPM5-MCs activated during chemical exposure could indirectly influence cell turnover by modulating the activity of SCs, which remove dead cells (Suzuki et al., 1996) and are hypothesized to regulate stem cell proliferation (Joiner et al., 2015). We hypothesize that the lack of TRPM5-MCs in *Skn-1a*<sup>-/-</sup> mice disrupts adaptive cholinergic modulation, leading to impaired MOE cell turnover and the olfactory deficits we previously observed after chemical exposure (Lemons et al., 2017). Notably, MCs expressing inositol triphosphate receptor subtype 3 (IP3R3-MCs; Elsaesser et al., 2005) promote MOE regeneration after tissue injury by stimulating cell proliferation (Jia et al., 2013), but it remains unclear whether this represents a conserved function among other MC subpopulations.

Factors regulating stem cell proliferation and cell turnover in response to chronic, mild chemical insults that often occur in nature and occupational settings are poorly understood, although MOE regeneration after drastic chemical lesion by various olfacto-toxicants is well demonstrated (Bergman et al., 2002; Xie et al., 2013). Additionally, inhaled chemicals impact the MOE in a region-specific manner due to the nasal anatomy and airflow (Kimbell et al 1997; Scott et al., 2014; Coppola et al., 2013, 2017) and there are substantial regional differences in cell turnover dynamics and tissue homeostasis (Vedin et al., 2009). However, associated regional differences in the adaptive maintenance of MOE structural and functional integrity are understudied.

In order to understand the factors contributing to the observed olfactory deficits in chemical-exposed *Skn-1a*<sup>-/-</sup> mice (Lemons et al., 2017), here we first systematically examined

MOE morphology in control and *Skn-1a*<sup>-/-</sup> mice after two-week chemical exposure and compared to those from vehicle (water) exposure groups. This is because several studies on inhalation or intranasal administration of harmful chemicals found that impaired olfactory function is often associated with epithelial damage and OSN loss (Jacquot et al., 2006; Kim et al., 2010; Jia et al., 2011), although we intended to avoid severe tissue damage by choosing a relatively mild chemical exposure. We then investigated whether TRPM5-MCs influence region-specific cell turnover by inhalation exposure of control TRPM5-GFP and *Skn-1a*<sup>-/-</sup> mice for two-weeks to either vehicle or chemicals. The chosen chemical exposure conditions challenged the MOE without inducing severe damage (Lemons et al., 2017). Our study provides the first evidence that adaptive changes in MOE cell proliferation and apoptosis and morphology occurring in response to two-week mild chemical exposure are region-specific and TRPM5-MC-dependent, further elucidating the important role of these cells in MOE protective maintenance.

## Experimental Procedures

### *Animals*

Adult male TRPM5-GFP (Clapp et al., 2006) and *Skn-1a*<sup>-/-</sup> mice (Matsumoto et al., 2011, Yamaguchi et al., 2014) aged 2-6 months were group housed (2-5 mice per cage) in a temperature and humidity-controlled facility with food and water available *ad libitum* for the duration of the exposure. *Skn-1a*<sup>-/-</sup> mice were generated through breeding pairs of homozygous knockouts, so there were no wild type littermates. In order to be consistent with our previous studies in this line of research (Lemons et al., 2017; Almatrouk et al., 2018), we used TRPM5-GFP mice which were bred in the same animal facility as our control mouse line because they provide visualization of TRPM5-MCs. The TRPM5-GFP mouse line is well established through many studies of nasal and other tissues throughout the body (Clapp et al., 2006; Lin et al., 2007; Saunders et al., 2013; Howitt et al., 2016). Under conventional housing conditions without additional chemical exposure, there are no statistically significant differences between TRPM5-GFP and *Skn-1a*<sup>-/-</sup> mice in odor-evoked electro-olfactogram responses or in the olfactory-guided behaviors that we tested (Lemons et al., 2017). We used only male mice because some of these mice were tested behaviorally in our previous study (Lemons et al., 2017), in which we used male mice to avoid variation due to the female estrous cycle. All experimental procedures were approved by the Institutional Animal Care and Use committee at the University of Maryland Baltimore County and carried out in accordance with the National Institute of Health Guide for the Care and Use of Laboratory Animals (NIH Publications No. 80-23) revised 1996.

### *Chemical exposure*

*Skn-1a*<sup>-/-</sup> and control TRPM5-GFP mice (hereafter referred to as control mice) were challenged with continuous exposure to inhaled chemicals for approximately one (7-8 consecutive days) or two (14-16 consecutive days) weeks in accordance with our previous protocols (Lemons et al., 2017). Briefly, a 10-15 mL glass vial containing a kimwipe soaked with 1mL of each of 4 odor solutions (ammonium hydroxide, ethyl acetate, propionic acid, and triethylamine at final concentrations of 0.019 M, 0.075 M, 0.083 M, and 0.013 M respectively) was placed in the home cage for the duration of the exposure period and refreshed daily. Mice were also exposed to fine chitin powder (Tokyo Chemical Industry Co., Ltd) for ten minutes daily by transferring them to an empty cage containing 0.25 g of powder and gently agitating the chitin powder with an air pump for the duration of the exposure. Control groups from both strains were exposed only to vehicle (water). To make our chemical exposure protocol more relevant to human health and occupational safety, we selected the odor chemicals based on their usage in commercial manufacturing applications and personal care and cleaning products as well as their reported ability to cause concentration-dependent nasal damage in rodents (Gaafar et al., 1992; Hardisty et al., 1999) and respiratory tract irritation in humans (U.S. National Library of Medicine Hazardous Substances Data Bank). Chitin is a major component of fungal cell walls and the exoskeletons of arthropods such as dust mites that is widespread in the natural environment and can be an allergen to the respiratory tract (Reese et al., 2007).

### *Tissue preparation*

Mice were sacrificed at the end of the exposure period and tissues were harvested according to our previously described methods (Lin et al., 2008, Ogura et al., 2011; Lemons et al., 2017). Briefly, mice were anesthetized by intraperitoneal injection with tribromoethanol (Avertin; 250 µg/g body weight) and sacrificed via perfusion fixation with phosphate buffered saline (PBS) containing 3% paraformaldehyde (PFA) with 19 mM L-lysine monohydrochloride, and 0.23% sodium m-periodate. Tissue was post-fixed for 60-90 minutes and placed in 25% sucrose in 0.1 M PBS overnight at 4°C. MOE tissue was dissected out using our published method for mouse nose deboning (Dunston et al., 2013) and embedded in Tissue-Tek Optimal Cutting Temperature medium (Sakura), with tissue from chemical-exposed mice and paired water-exposed mice embedded together to ensure the same processing conditions. Tissue blocks were cut in 14 µm coronal sections using a cryostat (Microm HM 550) and sections were mounted on plus charged slides (Globe Scientific Inc.) and stored at -80°C until use.

### *Immunohistochemistry*

Immunohistochemical staining was performed according to our previously published protocols used in the characterization of TRPM5-MCs (Lin et al., 2008; Ogura et al., 2011). Slides were thawed, rinsed in 0.1 M PBS at room temperature, and incubated in blocking buffer (2% normal donkey serum, 1% bovine serum albumin, 0.3% Triton X-100) for 1.5 hours at room temperature (RT) before incubating with primary antibodies at 4°C overnight. For certain antibodies, antigen retrieval treatment was performed prior to primary antibody incubation to achieve optimal labeling (Table 1). After primary antibody incubation, sections were rinsed in 0.1 M PBS, then incubated with secondary antibodies (1:400) for 1 hour at RT. The following secondary antibodies were used: Alexa Fluor 647 donkey anti-goat (Life technologies, A21447, RRID:AB\_2535864), Alexa Fluor 555 donkey anti-goat (Life technologies, A21432, RRID:AB\_2535853), Alexa Fluor 555 donkey anti-rabbit (Life technologies, A31572, RRID:AB\_162543), Alexa Fluor 647 donkey anti-rabbit (Life technologies, A31573, RRID:AB\_2536183), Alexa Fluor 488 donkey anti-chicken (Jackson ImmunoResearch, 703-545-155, RRID:AB\_2340375), and Alexa Fluor 647 donkey anti-mouse (Life technologies, A31571, RRID:AB\_162542). Slides were then rinsed in 0.1 M PBS, incubated with DAPI for 5 minutes (Sigma Aldrich, 0.29  $\mu$ M in 0.1M PBS), rinsed again in 0.1 M PBS followed by 0.1 M phosphate buffer (PB) and 0.05 M PB, and mounted with Fluoromount-G (SouthernBiotech). Tissues from mice in both exposure conditions and mouse lines were processed in parallel under the same conditions.

**Table 1. Primary antibodies used for immunohistochemical analysis.** Manufacturer information, working dilutions and antigen retrieval procedures for primary antibodies used in this study are listed. For heat-mediated antigen retrieval procedures, slides were immersed in the appropriate pre-heated antigen retrieval solution in a plastic coplin staining jar inside of a water bath for the stated amount of time.

| Antibody          | Host   | Company                   | Catalog # | Antigen retrieval  | Dilution |
|-------------------|--------|---------------------------|-----------|--|----------|
| Cleaved caspase-3 | Rabbit | Cell Signaling Technology | 9661      | 30 min @ 90°C in Dako target antigen retrieval solution (pH=9.0) | 1:2000   |



|  |         |                   |                                  |   |        |
|--|---------|-------------------|----------------------------------|---|--------|
| Growth associated protein 43 (GAP43)             | Rabbit  | Novus Biologicals | NB 110-89717SS, RRID:AB_10001196 | N/A   | 1:2000 |
| GFP  | Chicken | Abcam             | ab13970, RRID: AB_300798         | N/A   | 1:2000 |
| Ki67   | Rabbit  | Novus Biologicals | NB110-8971955, RRID:AB_1217074   | 10 min @ 90°C in 10 mM Na citrate (pH 6.0)    | 1:200  |
| NQO1 (NADPH:quinone oxidoreductase)              | Rabbit  | Sigma-Aldrich     | N5288, RRID:AB_1841045           | 3 min rinse @ RT in 0.01 M NaOH               | 1:500  |
| Opioid-binding and Cell Adhesion Molecule (OCAM) | Goat    | R&D Systems       | AF778, RRID:AB_2149710           | 3 min rinse @ room temperature in 0.01 M NaOH | 1:250  |
| Olfactory marker protein (OMP)                   | Goat    | Wako              | 544-10001, RRID:AB_664696        | N/A   | 1:1000 |

### *Image Acquisition*

Low magnification (10X) images for quantification analysis were taken on an Olympus BX 41 epifluorescence compound microscope equipped with a Retiga 4000R digital camera (Qimaging, British Columbia, Canada) and Qcapture Pro software (Qimaging). Exposure and gain were held consistent across imaging sessions. Higher magnification (20, 40, 60X) representative images were taken using an Olympus BX 61 epifluorescence microscope with a spinning disk confocal unit and Slidebook 5.0 software (3I, Denver, CO). Representative images were adjusted for brightness and contrast where necessary.

### *Quantitative morphological analysis*

For each animal, we analyzed both the anterior and posterior locations of the MOE by selecting at least two coronal MOE sections per location spaced approximately 280  $\mu\text{m}$  apart. Anterior MOE (aMOE) sections were defined as those sections where the VNO is present and posterior MOE (pMOE) sections were defined as those where endoturbinate IIa was present. Measurements and cell counts were taken in the dorsal recess, septum and endoturbinate II (posterior only) regions of each MOE section (See Figs. 1A-C & 6A-C for schematic drawings). Images were stitched together using the ImageJ grid stitching plugin with unknown configuration prior to measurement (Preibisch et al., 2009). Quantification of GFP positive (GFP+) TRPM5-MCs was performed manually. To measure the thickness of the epithelium and mature OSN layer in each section, three lines spaced 250-500  $\mu\text{m}$  apart were drawn perpendicularly from the basal lamina to the apical surface in each region, with the DAPI label used to define the basal lamina. Measurement of OMP+ OSN axon bundle size and quantification of cells or nuclei positively labeled with cleaved caspase-3 or Ki67 was performed using custom-made macros which incorporated the Yen (Yen et al., 1995), RenyiEntropy (Kapur et al., 1985) and Otsu (Otsu, 1979) thresholding algorithms, respectively, and analyze particles functions of ImageJ in batch processing mode, to facilitate measurement over large tissue areas in multiple MOE regions. Due to the large area of Ki67 immunoreactive (Ki67+) nuclei in some places, the randomness of their spatial distribution, and the tendency for labeled nuclei to be clumped in dense groups, we extracted and analyzed the percentage of thresholded epithelial area covered by Ki67+ nuclei (Ki67+ area percentage). Only nuclei above the basal lamina were included. We then used the area percentage to approximate the density of Ki67+ cells after determining the mean nuclei size from a random sample of Ki67+ nuclei. Quantification of immature OSNs (iOSNs) was conducted using a modified version of our line intensity scan analysis technique which uses hessian-based feature extraction to detect fluorescence peaks over the length of a line in images of fluorescently labeled tissue sections (Sathyanesan et al., 2012; [https://www.researchgate.net/publication/312593741\\_ImageJ\\_Line\\_scan\\_analysis\\_-\\_Including\\_Hessian\\_feature\\_detection\\_for\\_image\\_stacks](https://www.researchgate.net/publication/312593741_ImageJ_Line_scan_analysis_-_Including_Hessian_feature_detection_for_image_stacks)). A segmented line was drawn parallel to the apical surface of the MOE to intersect perpendicularly with the dendrites of fluorescently labeled GAP43+ iOSNs (see Fig. 8C inset), and the number of peaks identified along the length of the line using the Find Peaks function of BAR plugin for ImageJ (Ferreira et al., 2016) was used to calculate regional cell densities. The accuracy of all automated image analysis pipelines was verified by conducting manual analysis on a subset of images, and the output from each analysis was manually checked for accuracy. All analyses were conducted using NIH ImageJ software v1.52c.

### *Intracellular $\text{Ca}^{2+}$ ( $[\text{Ca}^{2+}]_i$ ) level measurement*

Resting  $[\text{Ca}^{2+}]_i$  levels of freshly isolated OSNs in Tyrode's saline were measured using  $\text{Ca}^{2+}$ -sensitive dye Fura-2AM as described in our previous publications (Ogura et al., 2011; Szebenyi et al., 2014; Fu et al., 2018). Briefly, mice were sacrificed with  $\text{CO}_2$  gas followed by cervical dislocation, and the turbinate portion of the MOE (pMOE) was dissected out and enzymatically treated with papain to dissociate OSNs, which were then loaded with 2 $\mu\text{M}$  Fura-2AM for about 20 min in Tyrode' saline containing (in mM): 140 NaCl, 5 KCl, 10 N-2-hydroxyethylpiperazine-N=2-ethanesulfonic acid buffer (HEPES), 1  $\text{MgCl}_2$ , 3  $\text{CaCl}_2$ , 10 Na pyruvate, and 10 D-glucose (pH 7.4). For measurement of resting  $[\text{Ca}^{2+}]_i$  levels, a pair of Fura-2 fluorescence images was captured every 3 sec at 340 and 380nm excitation lights using an inverted microscope (Olympus IX71) equipped with a UAPO/340 40x oil objective lens, a Hamamatsu cooled CCD camera (C9300-221), and a Sutter LS Xenon light source/filter changer controlled by Imaging Workbench software version 6 (INDEC BioSystems, Santa Clara, CA). We measured  $[\text{Ca}^{2+}]_i$  levels from the soma and knob regions of each OSN by averaging 30 sec (10 frames) of ratio fluorescence values from 340nm/380 nm excitation light images to estimate resting  $[\text{Ca}^{2+}]_i$  levels.

### *Experimental design and statistical analysis*

MOE morphology and cell density data from each anatomical region (e.g. anterior dorsal recess) was analyzed separately. Similarly, the resting  $\text{Ca}^{2+}$  levels of the dendritic knob and soma of individual OSNs were separately averaged within an experimental group. For morphology data, measurements from different sections from the same animal were averaged yielding one data value per animal. Scatter points on all bar graphs represent data values from individual animals and unless otherwise noted, sample sizes reported (n) represent the number of animals analyzed. Prior to ANOVA, the normality of the data residuals across groups was evaluated using the Shapiro-Wilk test. Data were analyzed using two-way analysis of variance (ANOVA) with between-subjects factors of mouse line and exposure condition followed by unprotected fisher's least significant difference test (Fisher's LSD) to conduct planned comparisons between water and chemical exposure conditions within a mouse line and between control and *Skn-1a*<sup>-/-</sup> mice in the water exposure condition. Normalized data values for the chemical-exposed groups were calculated by dividing the data value for each chemical-exposed animal within a mouse line by the mean of the corresponding water-exposed group. Student's *t*-test was used to compare normalized values between mouse lines within a given

region and between time points within a mouse line and region. If the F test for the equality of variances was significant, homogeneity of variance was not assumed and Welch's t test for unequal variances was used instead. If normality could not be assumed, Mann-Whitney U test was used. A Pearson product-moment correlation was used to analyze the relationship between epithelial and mOSN layer thickness in the aMOE after exposure. *P* values <0.05 were considered significant. IBM SPSS statistics 25 and GraphPad Prism 8 were used for statistical analysis and graphing. All data are expressed as the mean  $\pm$  standard error of the mean.

## Results

### **The posterior MOE (pMOE) of control and *Skn-1a*<sup>-/-</sup> mice remained morphologically intact after two-week chemical exposure**

In order to elucidate the mechanisms responsible for the significant functional deficits we previously observed in chemical-exposed *Skn-1a*<sup>-/-</sup> mice (Lemons et al., 2017), we systematically examined MOE morphology in control and *Skn-1a*<sup>-/-</sup> mice after two-week chemical exposure and compared to those from vehicle (water) exposure groups. The vast majority of the MOE is located posteriorly. Within the MOE, mature OSNs (mOSNs) contribute significantly to epithelial thickness (Costanzo & Graziadei, 1983). We measured the apical to basal thickness of the epithelium and olfactory marker protein (OMP)-expressing mature OSN (mOSN) layer in the dorsal recess, septum, and endoturbinates II regions of the pMOE (Fig. 1A & B). These medial regions were selected for analysis because they are centrally located along the respiratory passageway, likely leading to a more direct impact of inhaled chemicals (Kimbell et al., 1997; Scott, 2006; Schoenfeld & Cleland, 2005, 2006; Scott et al., 2014; Coppola et al., 2013, 2017). The MOE is roughly divided into four zones (Ressler et al., 1993; Vassar et al., 1993). To determine which zones our analysis regions belonged to, we immunolabeled MOE sections with two zonal markers. Dorsal zone 1 OSNs express the antioxidant enzyme NAD(P)H quinone dehydrogenase 1 (NQO1; Gussing & Bohm, 2004), while ventrolateral zones 2-4 house OSNs expressing olfactory cell adhesion molecule (OCAM; Yoshihara et al., 1997). As expected, the examined dorsal recess is exclusively within zone 1, while the septum and endoturbinates II analysis regions span both the NQO1+ zone 1 and OCAM+ zone 2 (Fig. 1C), indicating different zonal compositions among the three analysis regions.

Our measurement results show that following two-week exposure, pMOE and mOSN layer thickness were slightly reduced only in the dorsal recess of chemical-exposed control and *Skn-1a*<sup>-/-</sup> mice compared to water-exposed groups (Fig. 1D, representative images of the dorsal recess). Statistical analysis of pMOE and OMP+ mOSN layer thickness showed a significant

main effect of exposure condition on both measures only in the dorsal recess (Two way ANOVA, pMOE:  $F(1,32)=4.504$ ,  $p=0.042$ ; mOSN layer:  $F(1,31)=5.504$ ,  $p=0.026$ ). However, when analyzing the dorsal recess of either the control or *Skn-1a*<sup>-/-</sup> mouse line individually, there was no significant difference in pMOE thickness between chemical and water-exposed mice (Fig. 1E). When comparing the mOSN layer thickness between the chemical- and water-exposed groups within each mouse line, the decrease reached statistical significance in chemical-exposed *Skn-1a*<sup>-/-</sup> mice (Fig. 1F; *Skn-1a*<sup>-/-</sup>:  $p=0.047$ ; control:  $p=0.232$ , Fisher's LSD test). We did not find significant differences in pMOE or mOSN layer thickness between exposure groups in either the septum or endoturbinate (Fig. 1E & F). These quantitative results demonstrate that under our relatively mild chemical exposure conditions, there was no widespread morphological damage within the pMOE. Therefore, the physiological and behavioral deficits previously found in *Skn-1a*<sup>-/-</sup> mice after two-week chemical exposure are unlikely caused by MOE damage.

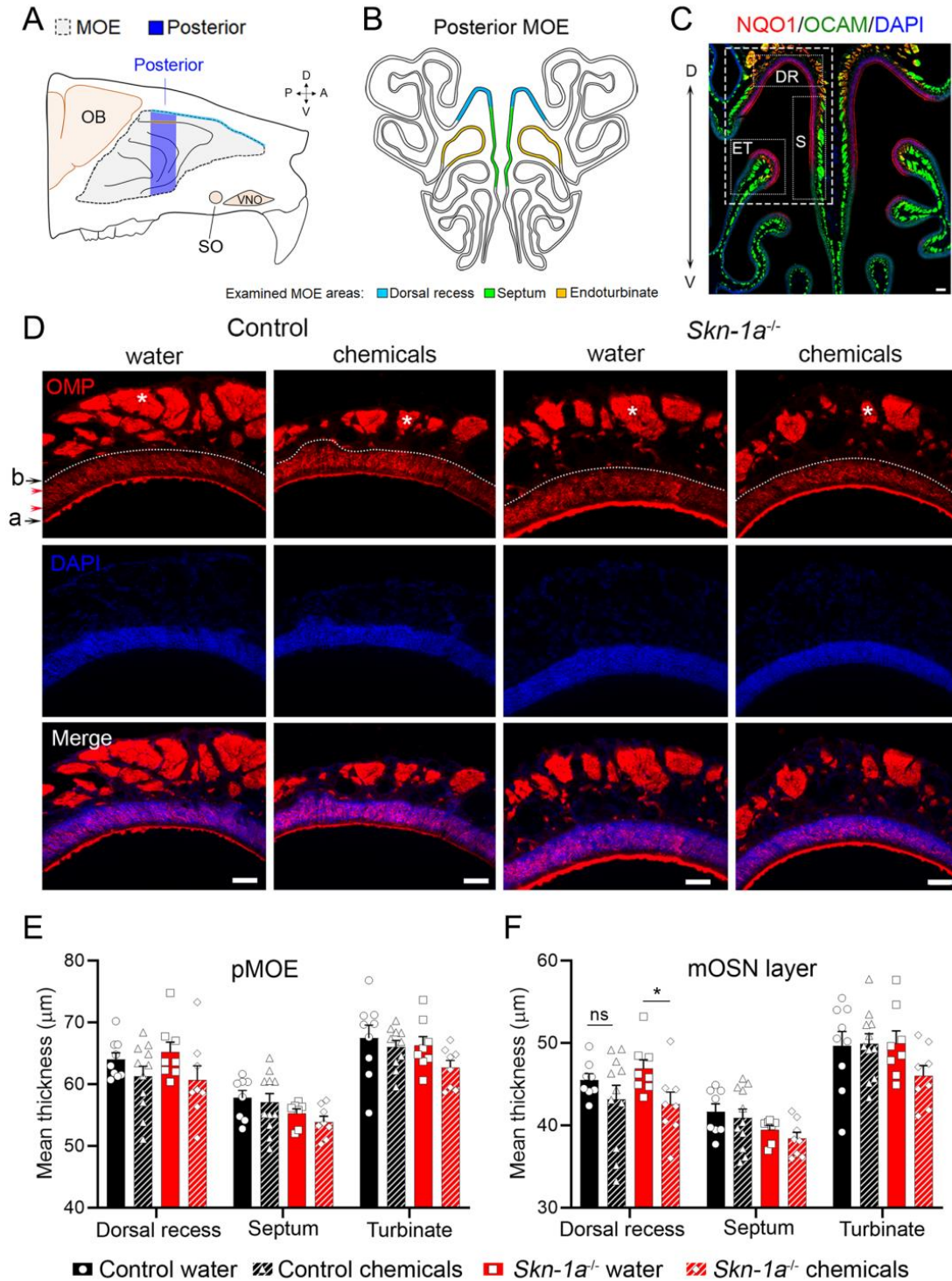


**Figure 1. Quantification of morphological changes in the pMOE of control and *Skn-1a*<sup>-/-</sup> mice after two-week exposure.** **A:** A midsagittal view of the mouse nasal structure, showing the entire MOE (gray, dashed outline) and posterior MOE (pMOE, blue) regions that were

analyzed after water or chemical exposure. SO: septal organ. VNO: vomeronasal organ. OB: olfactory bulb. **B**: A schematic representative section from pMOE. Sections of the pMOE were defined as those containing or immediately posterior to endoturbinate IIa. The dorsal recess, septum and endoturbinate IIa regions are indicated. **C**: A low magnification representative image of a pMOE section immunolabeled with zonal markers NQO1 (red) and OCAM (green) to visualize the dorsomedial zone 1 and ventrolateral zones 2-4, respectively. DAPI: nuclear stain (blue). Analysis regions are outlined with white dashed boxes (DR: dorsal recess; S: septum; endoturbinate: ET). D: dorsal, V: ventral. **D**: Representative OMP and DAPI labeling in the posterior dorsal recess of control and *Skn-1a*<sup>-/-</sup> mice after two-week exposure. Dashed line indicates the basal lamina and asterisks mark a representative OSN axon bundle in each OMP labeling image. In the upper left panel, black arrows point out the basal (b) and apical (a) surfaces of the epithelium as the start and end points for measurement of MOE thickness, while red arrowheads point out the basal and apical borders of the OMP-expressing mature OSN (OMP+ mOSN) layer as the start and end points for measurement of the mOSN layer thickness. **E** and **F**: Mean thickness of the pMOE (E) and the OMP+ mOSN layer (F) in the dorsal recess, septum and endoturbinate regions after exposure (control: n=8-11 mice/group; *Skn-1a*<sup>-/-</sup>: n=7-8 mice/group). p>0.05: not significant (ns). \*: p<0.05 in Fisher's LSD test following two-way ANOVA. Error bars: S.E.M. Scale: C, 100  $\mu$ m; D, 50  $\mu$ m.

### **Chemical exposure increased resting $[Ca^{2+}]_i$ levels in isolated OSNs of chemical-exposed *Skn-1a*<sup>-/-</sup> but not control mice**

The olfactory responsiveness measured via EOG depends on healthy OSNs population-wide in the pMOE. In our experience with  $[Ca^{2+}]_i$  imaging on isolated OSNs (Ogura et al., 2011, Szebenyi et al., 2014, Fu et al., 2018) and other chemosensory cells (Lin et al., 2008, Ogura et al., 2002; 2010), unhealthy cells generally exhibit a higher level of resting  $[Ca^{2+}]_i$  and die faster compared to healthy cells. Therefore, in order to evaluate the general health condition of OSNs after exposure, we enzymatically isolated OSNs lining the olfactory turbinates and measured their resting  $[Ca^{2+}]_i$  levels in the soma and dendritic knob regions using our established single-cell  $[Ca^{2+}]_i$  imaging technique (Ogura et al., 2011, Szebenyi et al., 2014). We identified isolated OSNs based on the characteristic morphology of their apical cilia (Ogura et al., 2011, Szebenyi et al., 2014). For the purpose of evaluating OSN health population-wide, we randomly measured OSNs and found that there was no statistical difference in average resting  $[Ca^{2+}]_i$  values estimated using Fura2 ratio in both the dendritic knobs and soma of OSNs between water-exposed control and *Skn-1a*<sup>-/-</sup> mice (Mann Whitney U-test, U=10284, p=0.9059 (Soma);

U=9598, p=0.2754 (Knob); n=144 (water) and 144 (chemicals); n=5 mice per group). When comparing the average resting  $[Ca^{2+}]_i$  level of OSNs of control mice between water and chemical-exposed groups, no statistically significant difference was found (Fig. 2A; control mice: water vs. chemicals: Mann Whitney U-test, U=9195, p=0.2006 (Soma); U=9914, p=0.8103 (Knob); n=144 (water) and 140 (chemicals), n=5 mice per group). However, OSNs of chemical-exposed *Skn-1a*<sup>-/-</sup> mice showed an increase in the average resting  $[Ca^{2+}]_i$  level compared to those of water-exposed *Skn-1a*<sup>-/-</sup> mice, although this trend did not reach statistical significance (Fig. 2D; *Skn-1a*<sup>-/-</sup> water vs. chemicals (Mann Whitney U-test, U=9695, p=0.2151 (Soma); U=9489, p=0.1269 (Knob); n=144 (water) and 147 (chemicals), n=5 mice per group). We further plotted the cumulative frequency to determine if there were differences in the distribution of  $[Ca^{2+}]_i$  levels between exposure conditions. In control mice, the resting  $[Ca^{2+}]_i$  levels exhibited a similar distribution frequency between water and chemical-exposed groups (Fig. 2B & C). However, the cumulative frequency distributions of water and chemical-exposed *Skn-1a*<sup>-/-</sup> mice were different at  $[Ca^{2+}]_i$  levels above an arbitrary unit of 0.75 (approximately 50% of the cumulative frequency value). There were more OSNs displaying an  $[Ca^{2+}]_i$  value in the lower range in the water-exposed group than the chemical-exposed group (Fig. 2E & F). To determine whether the difference was statistically significant, we compared the  $[Ca^{2+}]_i$  values from the upper 50% of OSNs with higher resting  $[Ca^{2+}]_i$  levels between water and chemical exposure groups. We found that there was a highly significant difference in OSNs of *Skn-1a*<sup>-/-</sup> mice [insets in Fig. 2E and F; Mann Whitney U-test, U=1959, p=0.0055 (Soma); U=1881, p=0.0020 (Knob); n=72 (water-exposed), 74 (chemical-exposed)], but no statistically significant difference was found in OSNs of control mice [insets in Fig. 2B & C; Mann Whitney U-test, U=2170, p=0.1530 (Soma); U=2392, p=0.6014 (Knob); n=72 (water-exposed), 70 (chemical-exposed)]. This physiological result indicates that chemical exposure negatively impacted the health condition of OSNs population-wide in the pMOE of *Skn-1a*<sup>-/-</sup> mice but not control mice.



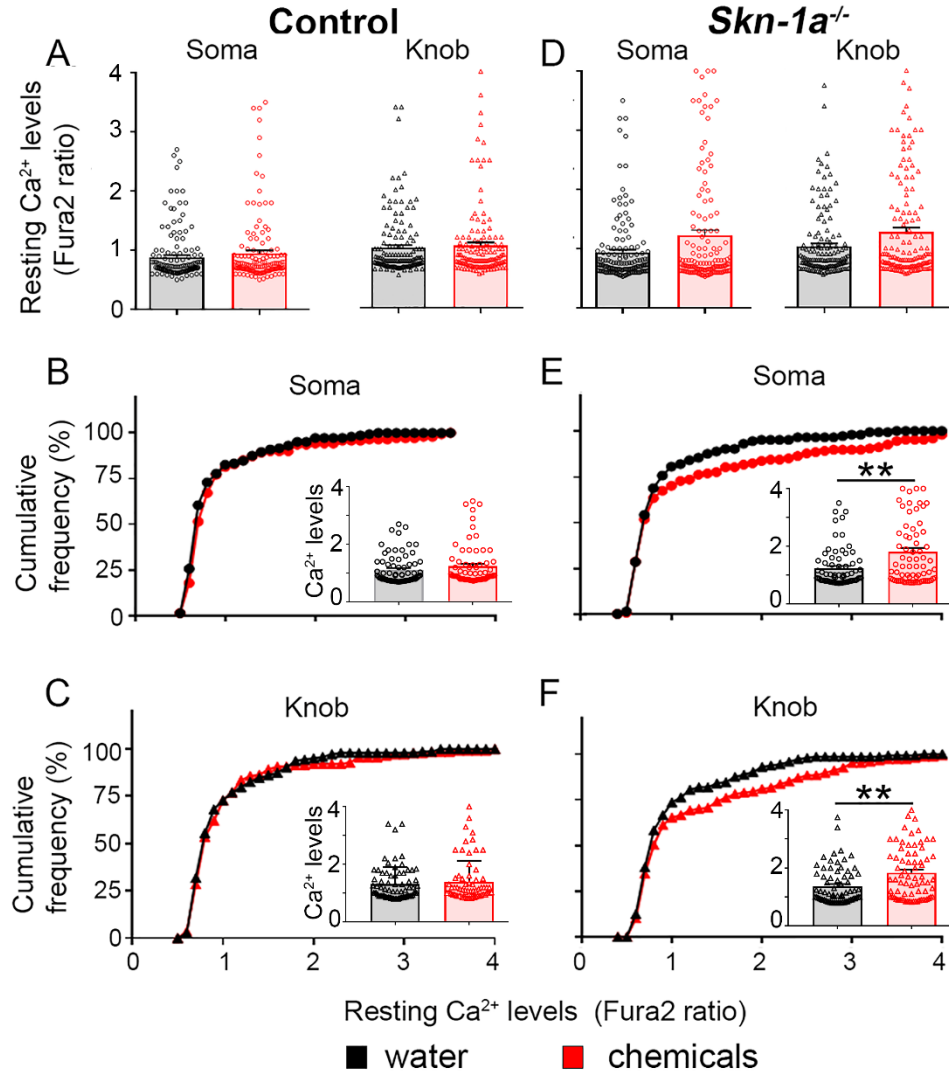


**Figure 2. Significant increase in resting intracellular  $\text{Ca}^{2+}$  levels of a subset of OSNs in *Skn-1a*<sup>-/-</sup>, but not control mice after two-week chemical exposure.** Resting intracellular  $\text{Ca}^{2+}$  levels of soma and knob regions of isolated OSNs from control (A-C) and *Skn-1a*<sup>-/-</sup> mice (D-F) were measured after two-week water (black) or chemical exposure (red). **A** and **D**: Plots of average resting  $\text{Ca}^{2+}$  levels. OSNs of chemical-exposed *Skn-1a*<sup>-/-</sup> mice showed higher average resting  $\text{Ca}^{2+}$  levels in both soma and knob regions compared to water-exposed mice [Mann Whitney U-test,  $p > 0.05$ ,  $n = 144$  (water) and 140 (chemicals) for control mice, 144 (water) and 147 (chemicals) for *Skn-1a*<sup>-/-</sup> mice,  $n = 5$  mice/group]. **B-C** and **E-F**: Cumulative histograms of resting  $\text{Ca}^{2+}$  levels in soma (●) and knob (▲) regions after two-week exposure. In control mice, OSNs from water- and chemical-exposed mice showed similar cumulative frequency of resting  $\text{Ca}^{2+}$  levels. A subset of OSNs from *Skn-1a*<sup>-/-</sup> mice exhibited higher resting  $\text{Ca}^{2+}$  levels ( $> 0.75$

Fura 2 ratio) compared to those of the water-exposed group. **Insets in B-C and E-F:** Plots of average resting  $\text{Ca}^{2+}$  levels of the upper 50% of OSNs that had higher resting  $\text{Ca}^{2+}$  levels. Chemical exposure significantly elevated the average resting  $\text{Ca}^{2+}$  levels in these OSNs of *Skn-1a*<sup>-/-</sup> mice in both soma and knob regions compared to those of water-exposed mice [Mann Whitney U-test \*\* $p < 0.01$ ,  $n = 72$  (water) and 70 (chemicals) for control mice, 72 (water) and 74 (chemicals) for *Skn-1a*<sup>-/-</sup> mice,  $n = 5$  mice/group].

### **Chemical exposure increased proliferating stem cells in the pMOE of control but not *Skn-1a*<sup>-/-</sup> mice**

Adult neurogenesis ensures the timely replacement of aged and damaged cells and preserves olfactory function (Calof et al., 1996). We next assessed the impact of chemical exposure on olfactory basal cell proliferation and determined whether this process is TRPM5-MC-dependent by using an antibody against Ki67 to immunolabel pMOE sections from both water- and chemical-exposed control and *Skn-1a*<sup>-/-</sup> mice. Ki67 is a nuclear protein expressed in proliferating cells (Gerdes et al., 1983; Scholzen & Gerdes, 2000). The vast majority of Ki67 immunolabeled (Ki67+) nuclei within the pMOE were located just above the lamina propria and unevenly distributed, some of which were clustered (Fig. 3A). We therefore measured the percentage of MOE area occupied by Ki67+ nuclei (the Ki67+ area percentage) and the associated epithelial area to evaluate the prevalence and distribution of Ki67+ proliferating cells in three regions of the pMOE (Fig. 3B: Right Y-axis). We also calculated the approximate cell density by estimating the number of cells within the selected pMOE area, which was done by measuring the size of individual Ki67+ nuclei through random sampling and dividing the total Ki67+ area by the average Ki67+ nuclei size (Fig. 3B, Left Y-axis). In addition, to better understand the time course of changes in MOE cell genesis, we performed this analysis at both the midpoint (one week) and endpoint (two weeks) of exposure (Fig. 3B). After one week of exposure, Ki67+ area percentage tended to increase in chemical-exposed control mice compared to water-exposed controls, although there were no statistically significant differences between exposure conditions in control or *Skn-1a*<sup>-/-</sup> mice (Fig. 3B, left). After two weeks of exposure, there was a significant main effect of exposure condition on Ki67 area percentage in endoturbinate II (Two way ANOVA,  $F(1,26) = 5.346$ ,  $p = 0.029$ ). However, when comparing between exposure conditions within each mouse line, only chemical-exposed control mice showed a significant increase in the Ki67+ area percentage compared to water-exposed control mice in the dorsal recess and endoturbinate II (Fig. 3B, right; [dorsal recess]  $p = 0.031$ , [endoturbinate]  $p = 0.034$ , Fisher's LSD test). In contrast, the Ki67+ area percentage was not

significantly different between water and chemical-exposed *Skn-1a*<sup>-/-</sup> mice across analysis regions of the pMOE at either time point.

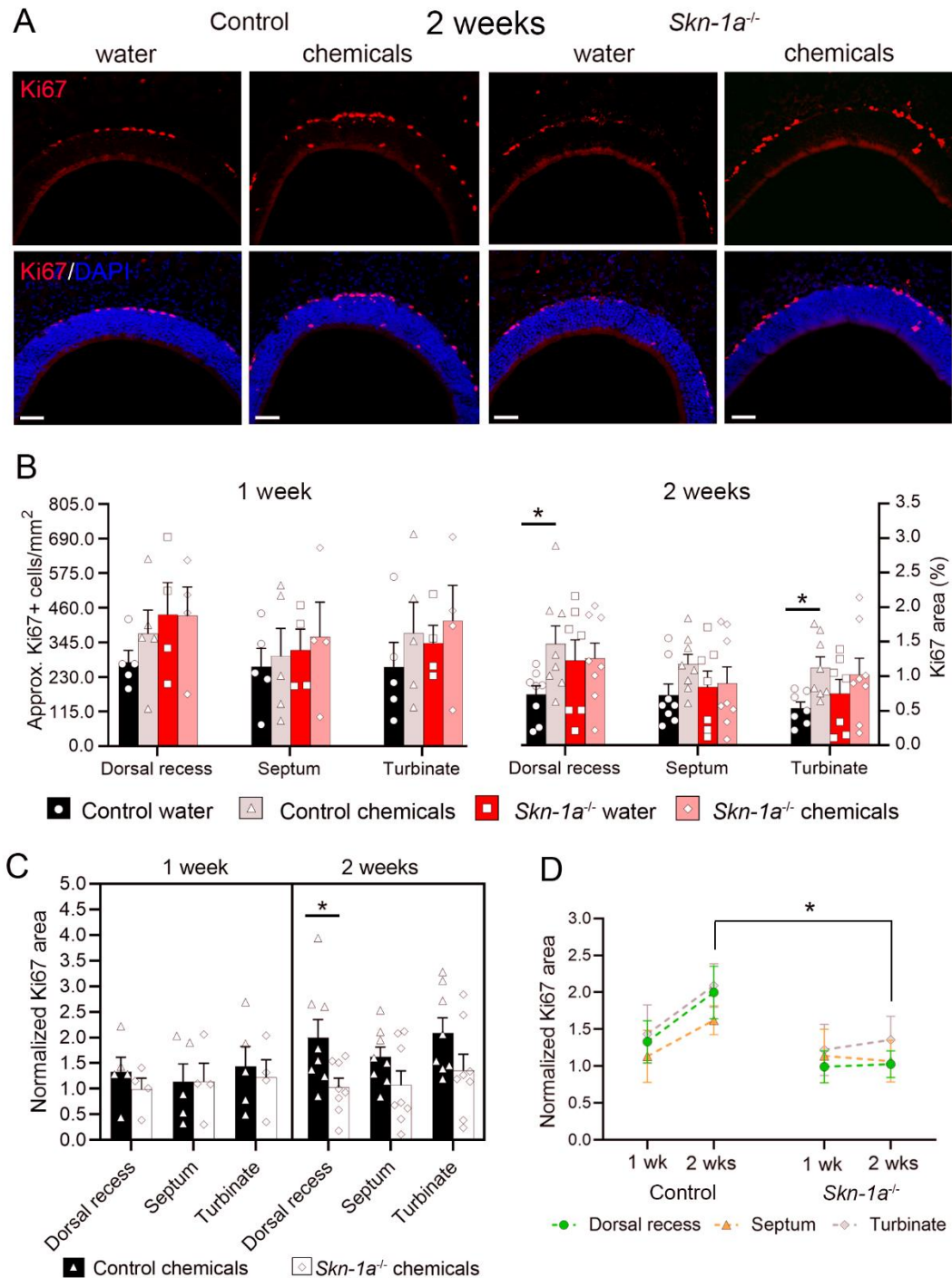


**Figure 3. Significant increase in cell proliferation in the pMOE of control but not *Skn-1a*<sup>-/-</sup> mice after two-week chemical exposure. A:** Ki67 immunolabeling in the dorsal recess of the

pMOE in two-week water and chemical-exposed mice. Scale = 50  $\mu$ m. **B:** Quantification of Ki67 immunolabeling across regions of the pMOE after one- and two-week exposure, respectively. The right Y axis indicates the mean percentage of the MOE area covered in Ki67+ nuclei. The approximate density of Ki67+ cells was calculated from the Ki67+ area percentage and is plotted on the left Y axis. \* $p < 0.05$ , Fisher's LSD test, 1 week,  $n = 4-5$  mice/group; 2 weeks,  $n = 7-8$  mice/group. **C:** Normalized Ki67+ area percentage in chemical-exposed mice relative to water-exposed mice of the same line after one and two weeks of exposure. \* $p < 0.05$ , Student's *t*-test, 1 week:  $n = 4-5$  mice/group, 2 weeks:  $n = 8$  mice/group. **D:** Normalized Ki67+ area percentage after one or two weeks of exposure. \* $p < 0.05$  in the dorsal recess, Student's *t*-test. Sample sizes same as in C. There were no significant differences detected between regions within a mouse line or between time points within a mouse line. Error bars: S.E.M.

In order to further evaluate the chemical exposure-induced changes between control and *Skn-1a*<sup>-/-</sup> mice, we normalized the Ki67+ area percentage obtained from the chemical-exposed groups to those of water-exposed groups of the same mouse line (Fig. 3C & D), since water-exposed *Skn-1a*<sup>-/-</sup> mice had a higher average Ki67+ area percentage across regions compared to water-exposed control mice in both the one-week and two-week exposure experiments (Fig. 3B). The normalized Ki67+ area percentage was significantly greater in chemical-exposed control mice than *Skn-1a*<sup>-/-</sup> mice in the dorsal recess after two-week chemical exposure (Fig. 3C & D; Student's *t*-test,  $t(14) = 2.43$ ,  $p = 0.029$ ) and remained consistently higher regardless of region or exposure duration, indicating that control but not *Skn-1a*<sup>-/-</sup> mice upregulated cell proliferation above the levels observed in water-exposed mice in response to chemical exposure. Additionally, the time course was different between chemical-exposed control and *Skn-1a*<sup>-/-</sup> mice. Chemical-exposed control mice showed a moderate increase in the normalized Ki67+ area percentage across regions between the midpoint and endpoint of exposure, although differences between time points within each region did not reach statistical significance. *Skn-1a*<sup>-/-</sup> mice showed no such time-dependent trend (Fig. 3D; Student's *t*-test,  $p > 0.05$ ). These findings indicate that chemical exposure stimulated a significant increase in stem cell proliferation in the pMOE which peaked after two weeks in control mice, but this adaptive increase in stem cell proliferation was lacking in the pMOE of chemical-exposed *Skn-1a*<sup>-/-</sup> mice.

**Chemical exposure did not globally increase cell death in the pMOE of control and *Skn-1a*<sup>-/-</sup> mice**

We next determined whether there was a significant change in cell death in the pMOE following the chemical exposure. Using an antibody against cleaved caspase-3 in immunolabeling, we quantified the number of caspase 3 positive (caspase 3+) apoptotic cells (Fig. 4). We focused on programmed cell death instead of necrosis because of the relatively mild chemical exposure conditions we used. The antibody labeled only a few cells in different regions of the pMOE in both control and chemical exposed conditions and these cells were randomly located with uneven distribution (Fig. 4A and B: representative images of caspase 3+ cells in the dorsal recess and endoturbinates II, respectively, of the pMOE in water-exposed mice). Also, the number of apoptotic cells in the pMOE of individual mice generally varied considerably. We found that apoptotic cell density was significantly greater in the posterior dorsal recess of chemical-exposed control mice compared to water-exposed control mice (Fig. 4C;  $p=0.032$ , Fisher's LSD test), but was not significantly different between water and chemical-exposed *Skn-1a*<sup>-/-</sup> mice (Fig. 4C). The difference in the normalized density of apoptotic cells between chemical-exposed control and *Skn-1a*<sup>-/-</sup> mice in the dorsal recess was borderline significant (Fig. 4D; Student's t-test,  $t(5)=2.511$ ,  $p=0.054$ ). These findings indicate that chemical exposure induced a small but significant regional increase in apoptosis in the dorsal recess of the pMOE in control but not *Skn-1a*<sup>-/-</sup> mice.

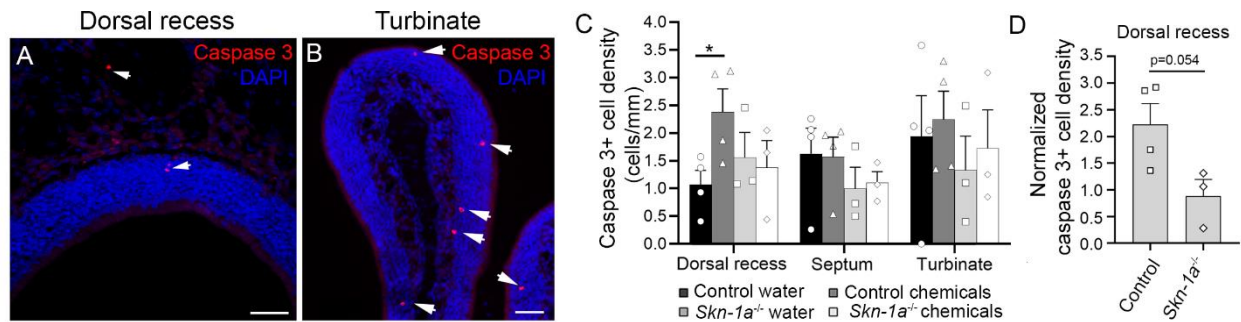


**Figure 4. Quantification of apoptosis in the pMOE after chemical exposure.** **A and B,** Representative cleaved caspase-3 and DAPI labeling the dorsal recess (**A**) and turbinate (**B**) of the pMOE in a water-exposed control mouse. Arrowheads point out positively labeled cells. Scale: 50  $\mu$ m. **C,** Density of caspase 3+ cells in the pMOE after two-week exposure, respectively, as counted along the length of the MOE surface (Fisher's LSD test: \* $p < 0.05$ ; n.s.: not significant;  $n = 3-4$  mice/group). **D,** Normalized density of caspase 3+ cells in the dorsal recess of chemical-exposed mice relative to water-exposed mice of the same line after two weeks of exposure. The difference in normalized cell density between control and *Skn-1a*<sup>-/-</sup> mice

was borderline significant at two weeks in Student's *t*-test,  $p=.054$ ,  $n=3-4$  mice/group. Error bars  $\pm$  SEM.

### **The TRPM5-MC population is maintained during chemical exposure but exhibits a regional difference in distribution along the anterior-posterior axis of the MOE**

It has been reported that the number of MCs is decreased in the regenerated MOE after two-week chronic inhalation exposure to the olfactory toxicants methyl bromide and nickel, which cause widespread MOE degeneration (Miller et al., 1995), and during aging in rodents (Kwon et al., 2005; Jia & Hegg, 2015). On the other hand, parasite infection increases the number of TRPM5-expressing chemosensory tuft cells in the digestive tract to engage immune responses (von Moltke et al., 2016; Gerbe et al., 2016; Howitt et al., 2016). The number of TRPM5-MCs in the MOE also increases regionally after X ray irradiation (Doyle et al., 2018). These findings indicate that MCs in the MOE and other TRPM5-expressing cells exhibit population-level plasticity in accordance with the conditions of the internal and external environment. From our previous studies, TRPM5-MCs are known to respond to the odor mixture used in our two-week chemical exposure (Fu et al., 2018) and other relatively high concentration volatile odors by increasing intracellular  $\text{Ca}^{2+}$  (Ogura et al., 2011). We therefore determined whether two-week chemical exposure alters the density of TRPM5-MCs by quantifying TRPM5-MCs in the dorsal recess, septum and endoturbinates II regions of both the pMOE and aMOE of water and chemical-exposed control (TRPM5-GFP) mice. GFP in the MOE of TRPM5-GFP mice is expressed in TRPM5-MCs and a subset of OSNs that are preferentially located in the lateral and ventral regions with very few in the dorsal recess (Lin et al., 2007). For accurate cell counts, we enhanced the GFP signal using an anti-GFP antibody and counted only TRPM5-MCs based on their distinct morphology and superficial location (Lin et al., 2007, 2008, Ogura et al., 2011, Yamaguchi et al., 2014). Representative images of TRPM5-MCs in the dorsal recess are shown in Fig. 5A-D. We noted some morphological and locational differences between the anterior and posterior TRPM5-MCs. Compared to TRPM5-MCs of the pMOE, TRPM5-MCs of aMOE displayed longer apical processes and their nuclei were mostly located in the nuclear layer of supporting cells instead of above it. We found no significant differences in TRPM5-MC density between exposure conditions in any of the regions under examination (Fig. 5E; Student's *t*-test,  $p>0.05$ ; endoturbinates II data not shown). Interestingly, the density of TRPM5-MCs was significantly greater in the dorsal and septum regions of the aMOE than in the corresponding regions of the pMOE in both water (Student's *t*-test, [dorsal recess]:  $t(12)=2.98$ ,  $p=0.011$ ; [septum]:  $t(10)=6.93$ ,  $p=0.000041$ ) and chemical-exposed TRPM5-GFP mice

(Student's *t*-test, [dorsal recess]:  $t(12)=2.93$ ,  $p=0.013$ ; [septum]:  $t(12.997)=5.163$ ,  $p=0.000183$ ). Chemical exposure did not significantly alter the regional differences in TRPM5-MC density (Fig. 5E; Student's *t*-test,  $p>0.05$ ). These findings confirm that our chemical exposure conditions did not damage TRPM5-MCs or reduce their number in the examined regions of the MOE. Our data further suggest that there is a graded regional distribution of TRPM5-MCs along the anterior-posterior axis of the MOE.

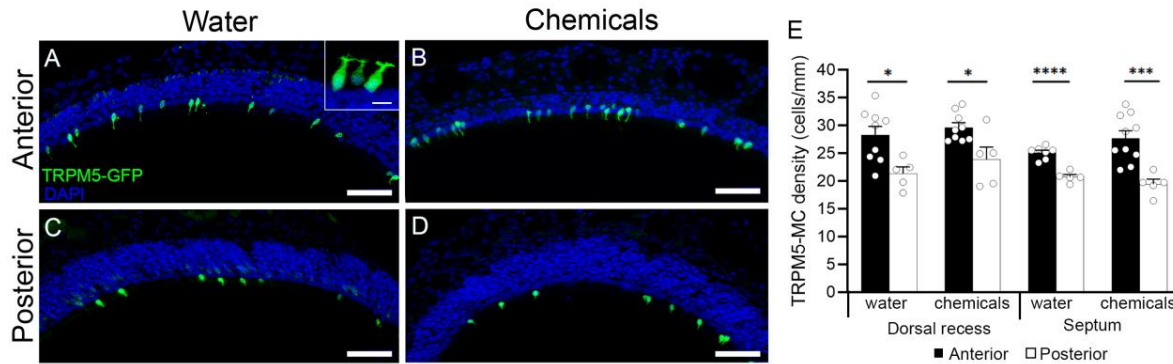


**Figure 5. TRPM5-MC density is significantly greater in the dorsal recess and septum of the aMOE compared to corresponding regions of the pMOE.** **A and B:** GFP+ TRPM5-MCs in the dorsal recess of the aMOE of TRPM5-GFP mice after two-week exposure to water or chemicals (inset in (A): higher magnification of TRPM5-MCs). **C and D:** GFP+ TRPM5-MCs in the dorsal recess of the pMOE of TRPM5-GFP mice after two-week exposure to water or chemicals. The GFP signal was intensified using an anti-GFP antibody. **E:** Mean density of TRPM5-MCs in the dorsal recess and septum of the aMOE versus pMOE of water and chemical-exposed mice as measured along the length of the MOE surface. TRPM5-MC density is significantly greater in the aMOE than the pMOE. Chemical exposure did not significantly alter the density of TRPM5-MCs in any region tested or the difference in the density between the aMOE and pMOE (Student's *t*-test, \*:  $p<0.05$ , \*\*\*:  $p<0.001$ , \*\*\*\*:  $p<0.0001$ ).  $n=7-10$  mice/group (aMOE),  $n=5$  mice/group (pMOE). Error bars: S.E.M. Scale: A-D: 50  $\mu$ m. Inset in A: 10  $\mu$ m.

### Chemical exposure induces substantial mature OSN loss and increased apoptosis in the aMOE of control but not *Skn-1a*<sup>-/-</sup> mice

To determine whether the higher density of TRPM5-MCs in the aMOE results in a greater impact on MOE morphology and plasticity, we extended our quantitative measurement of MOE and mOSN layer thickness to the anterior dorsal recess and septum regions (Fig. 6A-C,



schematics showing the aMOE and analysis regions). In contrast to the pMOE (Fig. 1C), the dorsal recess accounts for most of the aMOE surface area and the majority of OSNs in the aMOE are NQO1+ (Fig. 6D, white dashed box). Two-week chemical exposure generally led to a thinning of the aMOE and OMP+ mOSN layer in the dorsal recess region compared to water-exposed animals of the same mouse line (Fig. 6E). Unexpectedly, the thinning was markedly more severe in chemical-exposed control mice than *Skn-1a*<sup>-/-</sup> mice, sometimes even resulting in patchy areas lacking OSNs (Fig. 6E, chemical-exposed control). Since the MOE of the anterior septum region did not show substantial morphological changes in chemical-exposed mice of either mouse line (data not shown), we focused our quantification on the thickness of the dorsal recess aMOE and mOSN layer. When measuring the tissue thickness from water-exposed groups, we found that there was a strong, positive correlation between mean aMOE and mOSN layer thickness in the dorsal recess of both water-exposed control and *Skn-1a*<sup>-/-</sup> mice (Fig. 6F; control:  $r=0.921$ ,  $p=0.00016$ ; *Skn-1a*<sup>-/-</sup>:  $r=0.909$ ,  $p=0.00027$ ). The distribution of aMOE and mOSN layer thickness measurements was dramatically shifted toward the lower end of the data distribution in chemical-exposed control mice (Fig. 6F, red box), but the reduction in the aMOE and mOSN layer thickness remained highly correlated in both lines of chemical-exposed mice (Fig. 6F; control:  $r=0.879$ ,  $p=0.00036$ ; *Skn-1a*<sup>-/-</sup>:  $r=0.911$ ,  $p=0.001$ ), indicating that the reduced mOSN layer thickness constituted the main reason for the observed MOE thinning. Further, there were significant main effects of mouse line and exposure condition on the mOSN layer thickness, but not the aMOE thickness, in the anterior dorsal recess (Fig. 6G; two way ANOVA of mOSN layer thickness: [mouse line]  $F(1,36)=6.782$ ,  $p=0.013$ ; [exposure condition]  $F(1,36)=5.704$ ,  $p=0.022$ ). However, the mOSN layer thickness was significantly reduced only in chemical-exposed control mice compared to water-exposed controls (Fig. 6G; Control:  $p=0.010$ , *Skn-1a*<sup>-/-</sup>:  $p=0.450$ , Fisher's LSD test). Consistent with more extensive mOSN layer thinning, chemical-exposed control mice also concurrently exhibited a significant reduction in the size of the axon bundles visible beneath the basal lamina in the lamina propria (Fig. 6E) compared to the water-exposed group, whereas *Skn-1a*<sup>-/-</sup> mice did not (Fig. 6H; Two way ANOVA: ([mouse line]  $F(1,35)=0.009$ ,  $p=0.926$ ; [exposure condition]  $F(1,35)=14.76$ ,  $p=0.0005$ ; [interaction]  $F(1,35)=5.069$ ,  $p=0.031$ ; Control water versus chemicals:  $p=0.000076$ , *Skn-1a*<sup>-/-</sup> water versus chemicals:  $p=0.286$ , Fisher's LSD test). These results demonstrate that two-week chemical exposure induced more substantial OSN loss in the anterior dorsal recess of control than *Skn-1a*<sup>-/-</sup> mice and reveal a previously unknown role of TRPM5-MCs in MOE morphological plasticity.



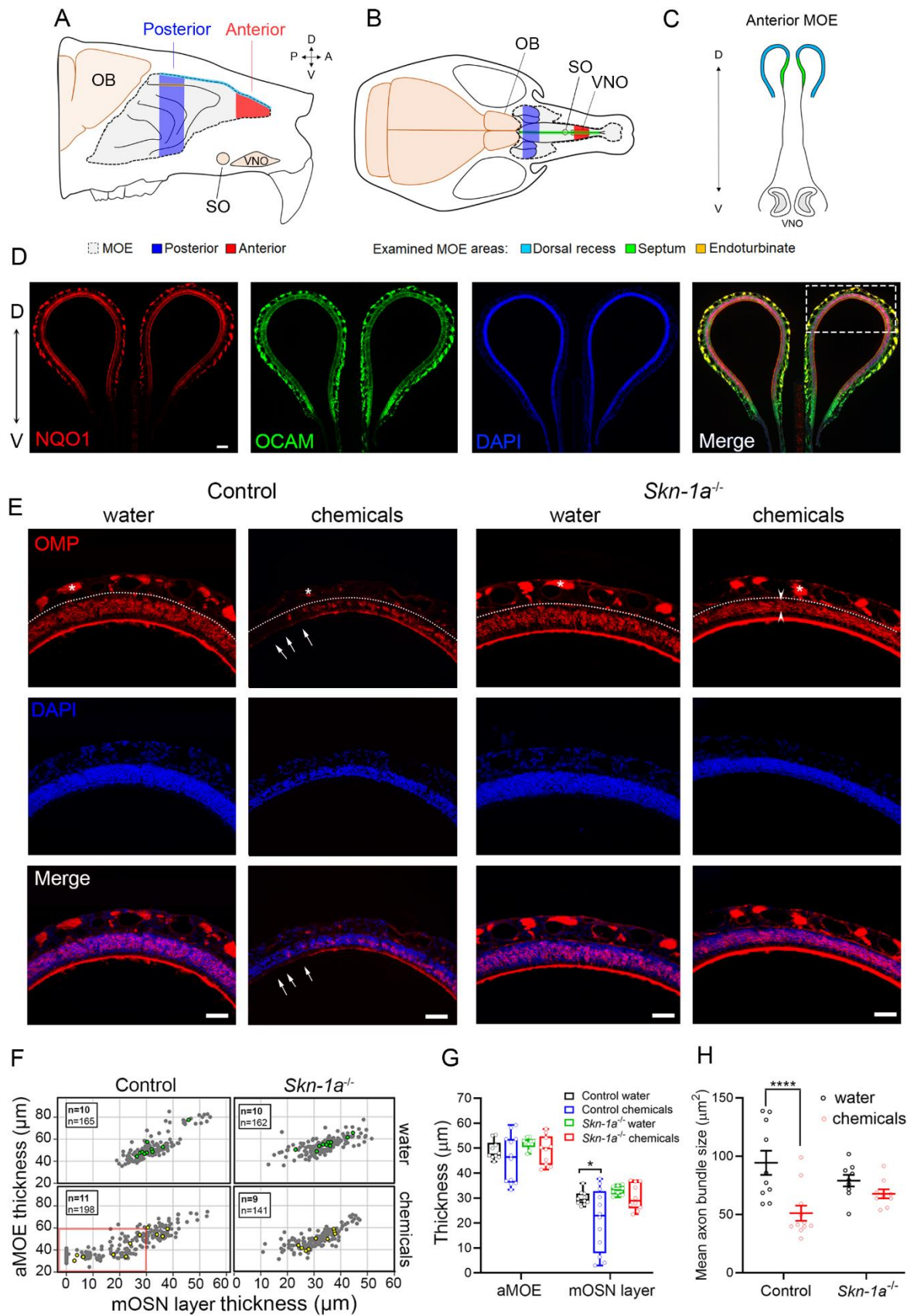


**Figure 6. Two-week chemical exposure induces greater loss of mature OSNs in the dorsal recess of the aMOE in control than *Skn-1a*<sup>-/-</sup> mice.** **A** and **B**: A midsagittal and dorsal views, respectively, of the mouse nasal structure, showing the aMOE (red) region for analysis. The pMOE is shown in blue for comparison. SO: septal organ. VNO: vomeronasal organ. OB: olfactory bulb. **C**: Schematic representative section of the aMOE. The aMOE sections were defined as those located directly above the VNO, anterior to the SO. **D**: Expression of zonal markers NQO1 (red, zone 1) and OCAM (green, zones 2-4) among mOSNs and axon bundles in the aMOE. The aMOE is dominated by NQO1+ OSNs (red). OCAM+ OSNs can be seen only in a small area of the most ventral portion of the aMOE region. The white dashed box in the merged panel indicates the location of the dorsal recess. D: dorsal, V: ventral. **E**: Representative images of OMP and DAPI labeling in the dorsal recess of control and *Skn-1a*<sup>-/-</sup> mice after two-week exposure. Dashed lines indicate the basal lamina and OSN axon bundles are marked with asterisks representatively. Arrowheads indicate the basal to apical neuronal layer thickness. Chemical-exposure results in more extensive thinning of the neuronal layer and reduction in OSN axon bundle size in the control mouse line than in the *Skn-1a*<sup>-/-</sup> line. Note the aneuronal area in the epithelium and the patchy spots missing DAPI stained nuclei in the chemical-exposed control mouse (point by arrows). Scale: D, 100  $\mu$ m; E, 40  $\mu$ m. **F**: Scatterplots showing measurements of the apical to basal thickness of the aMOE and OMP+ mOSN layer in the anterior dorsal recess after exposure. Three roughly equidistant measurements were taken from the left and right dorsal recess of each section (6 measurements/section). Each grey dot represents the average thickness within an individual section, while each colored dot represents the average thickness for an individual animal. More measurements cluster in the lower quadrant of the scatterplot in chemical-exposed control mice (red box) compared to water-exposed control mice. The total number of mice (bold) and total number of sections analyzed per experimental group are indicated in upper left of each panel. Each experimental group exhibited a significant positive correlation between aMOE and mOSN layer thickness after two-week exposure (Pearson correlation coefficient, Control water:  $r=0.921$ ,  $p=0.000155$ ,  $n=10$ ; *Skn-1a*<sup>-/-</sup> water:  $r=0.909$ ,  $p=0.000274$ ,  $n=10$ ; control chemicals:  $r=0.879$ ,  $p=0.000361$ ,  $n=11$ ; *Skn-1a*<sup>-/-</sup> chemicals:  $r=0.911$ ,  $p=0.001$ ,  $n=9$ ). **G**: Boxplots of the thickness of the aMOE and mOSN layer in the anterior dorsal recess generated from scatterplots in (F). Horizontal lines on each boxplot represent the median and quartiles and whiskers represent the data maximum and minimum values. Thickness of the mOSN layer is significantly reduced in chemical-exposed control mice compared to the water exposure group (Control water versus chemicals:  $p=0.010$ , *Skn-1a*<sup>-/-</sup> water versus chemicals:  $p=0.450$ , Fisher's LSD test). **H**: Quantification of the size of

OMP+ axon bundles in the lamina propria below the basal lamina. Mean axon bundle size is significantly reduced in chemical versus water-exposed control mice (Control water versus chemicals:  $p=0.000076$ , *Skn-1a*<sup>-/-</sup> water versus chemicals:  $p=0.286$ , Fisher's LSD test). Error bars: S.E.M. P values from Fisher's LSD test indicated as \*:  $p<0.05$ , \*\*\*:  $p<0.001$ , \*\*\*\*:  $p<0.0001$ .  $n=10-12$  control mice/group,  $n=8-9$  *Skn-1a*<sup>-/-</sup> mice/group.

To investigate whether chemical exposure-induced neuronal layer thinning in the aMOE progresses more quickly in *Skn-1a*<sup>-/-</sup> mice resulting in greater mOSN loss at an earlier time point, we performed the same analysis on mice exposed for one week. There were no statistically significant differences in aMOE or mOSN layer thickness between any of the experimental groups after one week of chemical exposure (Data not shown), excluding the possibility that the anterior OSNs of *Skn-1a*<sup>-/-</sup> mice turnover earlier than those of control mice during chemical exposure. These data also indicate that TRPM5-MC-mediated neuronal layer thinning in chemical-exposed control mice is time-dependent.

To investigate whether the OSN degeneration is mediated by programmed cell death, we immunolabeled aMOE sections with the anti-cleaved caspase 3 antibody. We found that chemical exposure induced a dramatic, time-dependent increase in apoptosis in the aMOE of control, but not *Skn-1a*<sup>-/-</sup> mice (Fig. 7A). There were significantly more apoptotic caspase 3+ cells in the aMOE of chemical-exposed control mice than in their water-exposed counterparts after one week (Fig. 7B; [dorsal recess] control water vs. chemicals:  $p=0.011$ , *Skn-1a*<sup>-/-</sup> water vs. chemicals:  $p=0.999$ ; [septum] control water vs. chemicals:  $p=0.026$ , *Skn-1a*<sup>-/-</sup> water vs. chemicals:  $p=0.921$ , Fisher's LSD test). The phenotype of increased apoptotic cells in the aMOE of chemical-exposed control mice could be observed as far anterior as the boundary with the respiratory epithelium. Caspase 3+ cell density remained moderately elevated in the dorsal recess of chemical-exposed control mice at the two-week time point (Note the difference in the Y-axis scales between one-week Fig. 7B and two-weeks Fig. 7C), but the difference between chemical and water-exposed control mice no longer reached significance (Fig. 7C; control water versus chemicals:  $p=0.087$ , *Skn-1a*<sup>-/-</sup> water vs. chemicals:  $p=0.718$ , Fisher's LSD test). In *Skn-1a*<sup>-/-</sup> mice, the density of caspase 3+ apoptotic cells between chemical and water-exposed groups was not significantly different at either time point in either region (Figs. 7B & C). Furthermore, the normalized cell density in the dorsal recess was significantly greater in chemical-exposed control than *Skn-1a*<sup>-/-</sup> mice at one week (Fig. 7D; Mann Whitney U-test,  $U=0.0$ ,  $p=0.029$ ). The time course of changes in apoptosis between one and two weeks in the aMOE was also different between control and *Skn-1a*<sup>-/-</sup> mice. In chemical-exposed control mice,

the normalized apoptotic cell density decreased between one and two weeks in both the dorsal recess and septum, with a significant difference in the dorsal recess (Fig. 7D; Mann Whitney U-test,  $U=0.0$ ,  $p=0.016$ ). In contrast, chemical exposure did not lead to a change in the normalized cell density between time points in either region in *Skn-1a*<sup>-/-</sup> mice (Fig. 7D; Student's *t*-test,  $p>0.05$ ).

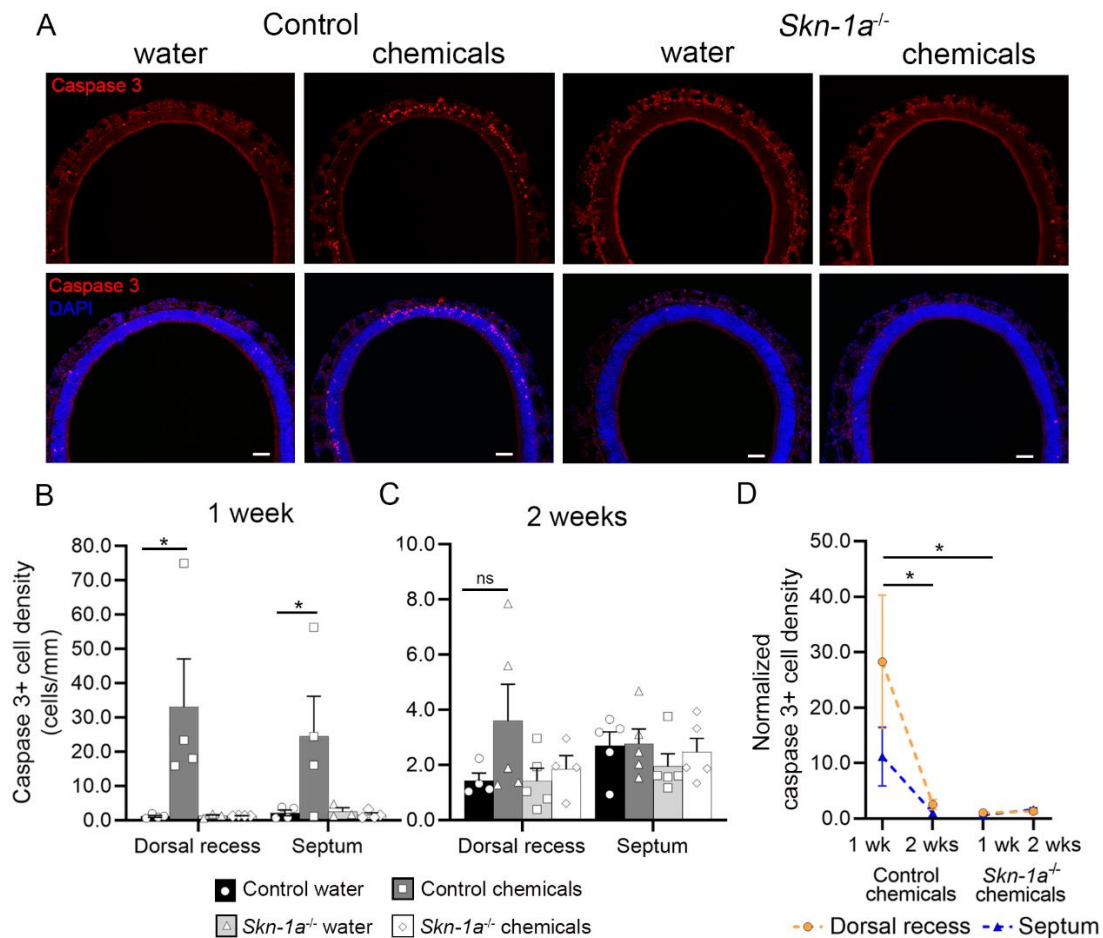


**Figure 7. Chemical exposure induces a time-dependent increase in the number of apoptotic cells in the aMOE of control but not *Skn-1a*<sup>-/-</sup> mice.** **A:** Cleaved caspase 3 immunolabeling for apoptotic cells and DAPI nuclear stain in the anterior dorsal MOE of control and *Skn-1a*<sup>-/-</sup> mice after one-week exposure. Scale: 60  $\mu$ m. **B** and **C:** Quantification of caspase 3 positive cells in the aMOE after one or two-week exposure, respectively. Two way ANOVA, one-week, dorsal recess: [mouse line]  $F(1,11)=4.283$ ,  $p=0.063$ ; [exposure condition]  $F(1,11)=4.356$ ,  $p=0.061$ ; [interaction]  $F(1,11)=4.348$ ,  $p=0.061$ ; septum: [mouse line]  $F(1,11)=3.116$ ,  $p=0.105$ ; [exposure condition]  $F(1,11)=2.817$ ,  $p=0.121$ ; [interaction]  $F(1,11)=3.341$ ,  $p=0.095$ .

Two weeks, dorsal recess: [mouse line]  $F(1,14)=1.107$ ,  $p=0.311$ ; [exposure condition]  $F(1,14)=2.438$ ,  $p=0.141$ ; [interaction]  $F(1,14)=1.082$ ,  $p=0.316$ ; P values from Fisher's LSD test indicated as: \*:  $p<0.05$ , \*\*\*:  $p<0.001$ , \*\*\*\*:  $p<0.0001$ , ns: not significant.  $n=3-4$  mice/group (one week),  $n=4-5$  mice/group (two weeks). **D:** Mean normalized density of caspase-3+ cells in chemical-exposed mice relative to water-exposed mice of the same line in the anterior dorsal recess or septum after one or two weeks of exposure. \*:  $p<0.05$ , Mann Whitney U-tests: Normalized caspase-3+ cell density in the dorsal recess of control vs. *Skn-1a*<sup>-/-</sup> mice after one-week chemical exposure,  $p=0.029$ ; Normalized cell density in the dorsal recess of control mice after one vs. two weeks of chemical exposure,  $p=0.016$ .  $n=4-5$  mice/group. Error bars: S.E.M.

### **Atrophic changes in the aMOE of chemical-exposed control mice do not stimulate basal cell proliferation or neurogenesis**

We expected that the substantial thinning and increased apoptosis in the aMOE of chemical-exposed control mice would stimulate basal cell proliferation and neurogenesis as part of regeneration during chemical exposure. Surprisingly, immunolabeling with the antibody against Ki67 (Fig. 8A) and subsequent quantitative analysis showed no significant increase in Ki67+ area percentage between water and chemical-exposed mice of either line in the aMOE after two-week exposure (Fig. 8B, right). Water-exposed control mice consistently showed a slightly higher Ki67+ area percentage than water-exposed *Skn-1a*<sup>-/-</sup> mice across regions and time points, with a significant difference in the septum at one week (Fig. 8B, left; Two way ANOVA, [mouse line]  $F(1,12)=12.30$ ,  $p=0.004$ ; [exposure condition]  $F(1,12)=1.866$ ,  $p=0.197$ ; [interaction]  $F(1,12)=8.346$ ,  $p=0.0136$ ; control water versus *Skn-1a*<sup>-/-</sup> water:  $p=0.0007$ , Fisher's LSD test). Also, the Ki67+ area percentage in the septum of chemical-exposed control mice was significantly decreased compared to the water-exposed control group at one week (Fig. 8B, left; control water vs. chemicals,  $p = 0.011$ , Fisher's LSD). There were no significant differences between water and chemical-exposed *Skn-1a*<sup>-/-</sup> mice at the one-week time point. Furthermore, we performed GAP43 immunolabeling and quantification after two-week exposure in the anterior dorsal recess and found that there was no significant difference in the density of GAP43+ immature OSNs (iOSNs) between water and chemical exposure groups in either mouse line (Fig. 8C). In sum, the TRPM5-MC-dependent increase in apoptosis and thinning of the neuronal layer in the aMOE during chemical exposure was not associated with an increase in adult neurogenesis.

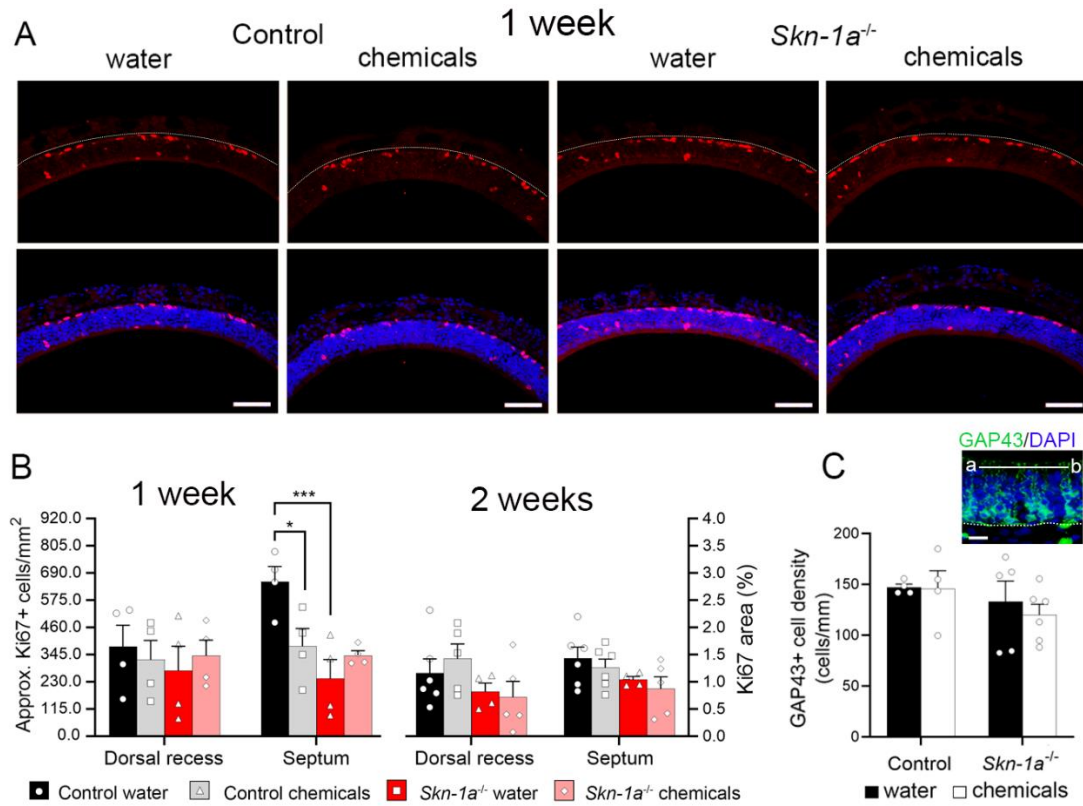


**Figure 8. No significant increase in cell proliferation and neurogenesis in the aMOE of chemical-exposed mice. A:** Ki67 immunolabeling in the dorsal recess of the aMOE in one-week exposed mice. The dashed lines in each panel mark the basal lamina. Only cells located above the basal lamina were counted. Scale: 50 μm. **B:** Quantification of Ki67+ cells in different regions of the aMOE after one (n=4 mice/group) and two (n=4-6 mice/group) week exposure. The right Y axis indicates the mean percentage of the epithelial area covered in Ki67+ nuclei. The left Y axis indicates the corresponding approximate density of Ki67+ cells, which was calculated from the Ki67+ area percentage. P values from Fisher's LSD test indicated as: \*: p<0.05; \*\*\*: p<0.001. **C:** Density of GAP43 immunoreactive (GAP43+) iOSNs in the anterior dorsal recess was not significantly different between exposure groups after two-week chemical exposure (control water vs. chemicals, p=0.9586, *Skn-1a*<sup>-/-</sup> water vs. chemicals, p=0.5154, Fisher's LSD test). n=4 control mice/group, n=5 *Skn-1a*<sup>-/-</sup> water, n=6 *Skn-1a*<sup>-/-</sup> chemicals. Inset: GAP43 immunolabeling of iOSNs with DAPI nuclear stain from the dorsal recess region of a water-exposed control mouse. The dotted line marks the basal lamina. The line at the superficial region of the MOE illustrates the location of the line intensity scan analysis used for quantifying GAP43+ dendrites. Scale: 25 μm. Error bars: S.E.M.

## Discussion

We have provided evidence for the involvement of TRPM5-MCs in coordinating region-dependent morphological plasticity through comparative and quantitative analyses. Our data showed that *Skn-1a*<sup>-/-</sup> mice lacking TRPM5-MCs failed to upregulate cell proliferation in the majority of the MOE located posteriorly, which potentially led to compromised health of the OSN population during two-week chemical exposure. We also showed that there is significant epithelial remodeling through tissue thinning and caspase 3-mediated apoptosis in the aMOE which occurs in an exposure duration-dependent fashion, and that TRPM5-MCs influence the extent of these alterations. Together, our findings underscore the importance of MCs in MOE adaptive plasticity and expand our current understanding of the TRPM5-MC-dependent MOE regulatory network that preserves odor responsiveness and olfactory-guided behavior under challenging chemical environments (Lemons et al., 2017).

Overall, our results uncover distinctly different mechanisms that adaptively maintain olfactory epithelial integrity and function between the aMOE and pMOE. Inhaled air flows through the rodent nasal cavity in distinct anterior-posterior and dorsomedial-ventrolateral airflow gradients (Kimbell et al., 1997; Scott et al., 2014; Coppola et al., 2017), such that the airflow is comparatively higher in the anterior and dorsomedial domains (primarily zone 1) along the respective axes. The aMOE is almost entirely composed of the dorsal recess, which includes only zone 1. Interestingly, OSNs of the zone 1 dorsomedial MOE are longer-lived with a slower turnover rate than those of the ventrolateral MOE (Vedin et al., 2009). They also possess more and longer cilia resulting in higher odor sensitivity (Challis et al., 2015), and exhibit greater OR diversity than OSNs in ventrolateral zones 2-4 (Zhang et al., 2004; Schoenfeld & Cleland, 2005). These combined anatomical and cellular properties may increase the anterior OSNs' susceptibility to environmental chemical insults. Thus, the loss of OSNs without a corresponding increase in basal cell proliferation in the aMOE in response to chronic chemical exposure might present an adaptive mechanism. The resulting reduction in the MOE area would minimize the potential inflammation associated with neuronal death, which might be beneficial for the health of the nasal mucosa and the central olfactory system (Pozharskaya et al., 2013; Kim et al., 2019). The functional redundancy in the olfactory system likely enables such an adaptive change to occur without significantly compromising overall function, as observed in our previous physiological and behavioral studies (Lemons et al., 2017).

Our findings in the olfactory system agree with recent reports that show TRPM5-expressing intestinal tuft cells coordinate the epithelial defense network and remodeling in response to parasitic infection, and the absence of such adaptive changes in *Skn-1a*<sup>-/-</sup> mice



lacking these cells (Gerbe et al., 2016; Schneider et al., 2018). Similar atrophic morphological changes have also been reported in the MOE of mice exposed to cigarette smoke solutions (Ueha et al., 2016a, 2016b) and aged rodents and humans (Loo et al., 1996; Doty and Kamath, 2014; Ueha et al., 2018). Thus, the aMOE tissue remodeling is likely not specific to our chemical treatment. Instead, it may represent a common outcome of chronic mild environmental exposure. In support of the involvement of TRPM5-MCs, we found that the density of TRPM5-MCs is significantly higher in the aMOE than the pMOE, which mirrors the anterior-posterior airflow gradient through the nasal cavity, further supporting the role of TRPM5-MCs' activity in the generation of regionalized responses to chemical exposure.

In stark contrast to the aMOE, we found increased proliferation in the pMOE of chemical-exposed control but not *Skn-1a*<sup>-/-</sup> mice. The pMOE accounts for the vast majority of MOE surface area and is dominated by the OCAM+ ventrolateral zones 2-4 spanning the septum and turbinates. The zone 1 dorsal recess accounts for only a small area of the pMOE. Due to the airflow gradients and hydrophilic nature of the odor mixture used in our two-week exposure, we expected the pMOE to receive a lower level of chemical exposure impact than the aMOE, which our results indicate was not enough to induce widespread tissue damage but was sufficient to stimulate proliferation of stem cells. The biological significance of this increase in cell proliferation is that it allows the MOE to replace OSNs that were worn-out during chemical exposure and thereby contributes to TRPM5-MC-mediated olfactory functional maintenance discovered in our previous study (Lemons et al., 2017). In support of this notion, we found that OSNs of chemical-exposed control mice maintained their average resting  $[Ca^{2+}]_i$  level using  $Ca^{2+}$  imaging, while a subset of OSNs of chemical-exposed *Skn-1a*<sup>-/-</sup> mice showed unhealthily high levels of intracellular resting  $[Ca^{2+}]_i$  indicating compromised  $Ca^{2+}$  homeostasis.  $[Ca^{2+}]_i$  plays a critical role in olfactory signal transduction adaptation, termination and other cellular processes and is highly regulated (Zufall et al., 1991; Reisert et al., 2003; Stephan et al., 2011; Szebenyi et al., 2014). Therefore, our findings from the pMOE are significant because the data reveal novel, TRPM5-MC-mediated region-specific adaptive modulation of adult cell genesis, which is known to be important for MOE structural and functional maintenance.

How might TRPM5-MCs influence pMOE cell proliferation for epithelial maintenance during chemical exposure? TRPM5-MCs are derived from the same transcription factor *Ascl3*+ progenitors as IP3R3-MCs (Weng et al., 2016). While IP3R3-MCs possess a basal process and may directly stimulate basal stem cell (BC) proliferation and neurogenesis through release of NPY both for normal tissue homeostasis and after injury (Montani et al., 2006; Jia et al., 2013; Pfister et al., 2015), TRPM5-MCs lack a basal process, making it unlikely that they directly



modulate basal cell proliferation. However, as we previously demonstrated, TRPM5-MCs are cholinergic and ACh application led to significant increases in intracellular  $\text{Ca}^{2+}$  levels and endocytotic activity in neighboring SCs (Ogura et al., 2011; Fu et al., 2018). SCs physically surround OSNs' cell bodies and dendrites and also possess a basal process (endfoot) which extends to the basal lamina to mingle amongst BC populations (Joiner et al., 2015). Because of the close anatomical relationships between SCs and OSNs and BCs, SCs have been hypothesized to contribute to MOE maintenance and plasticity by influencing the development and function of these neighboring cell populations through the paracrine release of modulators such as neurotrophic growth factors (Simpson et al., 2003), which regulate a wide range of cellular activities such as proliferation, neuronal survival, death and structural plasticity in the olfactory mucosa and the nervous system (Carter & Roskams, 2002). Joiner and colleagues recently demonstrated that the primary cilia of horizontal basal cells (HBCs) closely appose SC endfeet and loss of HBC cilia impairs MOE regeneration after methimazole lesion, furthering evidence for a functional connection between SCs and BCs (Joiner et al., 2015). HBCs are normally quiescent and only become active upon severe epithelial degeneration (Leung et al., 2007; Iwai et al., 2008), making them an unlikely candidate underlying the increased proliferation observed under our chemical exposure conditions. Nonetheless, these findings support the idea of a functional connection between SCs and BCs which may play into our results. Secreted growth factors act as important signaling molecules that regulate the timing and rate of occurrence of basal cell proliferation and neuronal precursor differentiation in the MOE (Gokoffski et al., 2010). Based on our current and previous results, we speculate that cholinergic modulation of SC activity may represent a novel avenue by which TRPM5-MCs simultaneously 1) communicate with BCs indirectly to regulate the release of signaling mediators important for OE maintenance and repair from SCs; and 2) upregulate other protective and maintenance functions of SCs during environmental challenge, such as phagocytosis of dead cells and debris and xenobiotic metabolism (Suzuki et al., 1996; Ding & Dahl, 2003; Kudo et al., 2010; Thiebaud et al., 2011; Fu et al., 2018). In this scenario, the lack of TRPM5-MCs in the MOE intercellular network of *Skn-1a*<sup>-/-</sup> mice could lead to an insufficient adaptive increase in cell proliferation and impaired epithelial maintenance during chemical exposure, which compromises the health of the epithelium and results in the previously identified functional deficits (Lemons et al., 2017).

Neurotrophic factors (NTs) may also play a role in the observed phenotypes. NTs are growth factors that are important for cell development, survival, function and injury-induced plasticity in the olfactory system and in the nervous system at large (Carter & Roskams, 2002).

In a concurrent study, we quantitatively analyzed the gene transcript expression of NTs and NT receptors (NTRs) in the MOE and MOB of control and *Skn-1a*<sup>-/-</sup> mice after two-week water or chemical exposure. We found that the gene expression of p75NTR, a pan neurotrophin receptor was significantly increased in the MOE of *Skn-1a*<sup>-/-</sup> mice but decreased in control mice after two-week chemical exposure compared to water-exposed group of the same mouse line (Almatrouk et al., 2018). The p75 (NTR) is activated by various NTs to form complexes that regulate a wide range of neuronal activities such as neuronal survival and neurite outgrowth during regeneration (Barker, 2004; Meeker & Williams, 2014; Chakraborty et al., 2017). We also found regional cell type specific localization of the p75NTR immunolabeling in the MOE, with a p75NTR antibody labeling BCs in the aMOE and SCs in ventral and lateral parts of the pMOE in addition to the olfactory ensheathing cells (Almatrouk et al., 2018). This TRPM5-MC-dependent downregulation of p75NTR expression and regional difference in the cellular localization of p75NTR may contribute to the phenotypes reported here by adaptively decreasing OSN generation and survival in specific regions of the control mouse MOE. Conversely, the upregulation of p75NTR expression in chemical-exposed *Skn-1a*<sup>-/-</sup> mice may contribute to an enhanced survival of unhealthy OSNs due to chronic activation during chemical exposure and lack of timely replacement by BCs.

The MOE, and especially SCs, carries out the metabolism and clearance of xenobiotics and odor molecules through the expression of various xenobiotic metabolizing enzymes (XMEs) and transporters such as cytochromes P450, glutathione S transferases, multidrug resistance transporters (Miyawaki et al., 1996; Whitby-Logan et al., 2004; Heydel et al., 2019). XMEs have been demonstrated to alter EOG responses and odor perception (Thiebaud et al., 2013; Nagashima and Touhara, 2010; Asakawa et al., 2017). Expression of XMEs also varies zonally in the MOE (Miyawaki et al., 1996; Whitby-Logan et al., 2004), suggesting that in addition to zonal and regional differences in receptor distribution and cell turnover activity (Vassar et al., 1993; Loo et al., 1996; Vedin et al., 2009), different MOE regions likely have varying capacities for chemical metabolism and clearance as well. We have previously demonstrated the strong effects of cholinergic modulation on SCs, with ACh increasing intracellular Ca<sup>2+</sup> levels and endocytosis in SCs via the muscarinic ACh receptor type 3 (Ogura et al., 2011; Fu et al., 2018). The chemicals we used for our exposure are exogenous chemical stimuli, which can be considered xenobiotics. We have shown that the odor mixture stimulates an increase in intracellular Ca<sup>2+</sup> levels in TRPM5-MCs (Fu et al., 2018). It is possible that TRPM5-MC activation during chemical exposure leads to subsequent release of ACh and potentially other

substances to upregulate the capacity for xenobiotic metabolism in SCs to promote clearance of these odor irritants in the mucus and minimize chronic overstimulation of OSNs.

Based on our data, we expect that other mechanisms besides TRPM5-MCs regulate cell turnover activity and epithelial maintenance both during environmental challenge and under basal conditions in *Skn-1a*<sup>-/-</sup> mice. Both lines of mice exhibited epithelial and mOSN layer thinning in the aMOE after two-week chemical exposure, although it was much more severe in control mice. This suggests that TRPM5-MCs are not necessary for initiating OSN loss but are important for influencing the extent of this phenotype. Since the *Skn-1a* transcription factor is not expressed by TRPM5 negative MCs such as IP3R3-MCs, these cells are still present in the MOE of *Skn-1a*<sup>-/-</sup> mice (Yamaguchi et al., 2014) and may also be activated by chemical exposure as they are chemoresponsive (Hegg et al., 2010). Therefore, their potential contribution to the reported phenotypes cannot be excluded. It is possible that BC proliferation may be redundantly regulated by both MC subpopulations such that loss of one MC cell type does not completely diminish MC's overall role in MOE maintenance.

Since we chose relatively mild odorous irritants for the exposure, the increase in cell proliferation in the pMOE and atrophic changes in the aMOE of control mice are expectedly less pronounced than those produced by known olfactotoxicants (Bergman et al., 2002; Xie et al., 2013). In agreement with this, we did not find a significant global increase in the number of caspase 3-positive apoptotic cells and GAP43-positive iOSNs in the pMOE following the two-week exposure (data not shown), which would have been suggestive of ongoing regeneration from damage. However, understanding mechanisms employed by the olfactory system in response to relatively mild odorous irritant exposure is important since a wide variety of such exposures can take place in occupational and industrial settings, in poorly ventilated buildings and shops, or in situations where people are subject to second-hand exposure to smoke or vapor from various tobacco products. In this aspect, our more moderate results actually reveal the MOE's capability of adaptive maintenance.

In sum, our study discovered two distinctive TRPM5-MC-dependent and MOE region-specific adaptive mechanisms occurring in response to chronic mild chemical challenge. Our findings further suggest that TRPM5-MC-mediated modulation of MOE morphology and proliferation is shaped by both nasal anatomy and intrinsic regional differences in homeostatic maintenance. In light of our previous results showing that olfactory responses are preserved in control, but not *Skn-1a*<sup>-/-</sup> mice during the same chemical exposure, we suggest that the TRPM5-MC-dependent upregulation of olfactory stem cell proliferation is biologically important for functional maintenance of OSNs in challenging chemical environments.

**Author contributions:** KL performed all the morphological and quantitative experiments, data analyses, and drafted most of the manuscript. ZF and TO performed intracellular Ca<sup>2+</sup> imaging, data analysis and drafted the results. WL conceived and supervised the project and participated in manuscript writing. All authors read, edited and approved the manuscript.

**Acknowledgements:** This work was supported by NIH/NIDCD DC012831 to W. Lin. We thank Drs. Robert Margolskee and Ichiro Matsumoto for breeding pairs of TRPM5-GFP and Skn-1a knockout mice, respectively. We also thank Dr. Jeff Leips for guidance on statistical analysis, Dr. Aaron Sathyanesan for advice on line intensity scan analysis, and Ms. Fenge Ni and Prasiddha Ramachandran for technical assistance.

## References

- Almatrouk A, Lemons K, Ogura T, Luo W, Wilson C, Lin W (2018) Chemical exposure-induced changes in the expression of neurotrophins and their receptors in the main olfactory system of mice lacking TRPM5-expressing microvillous cells. *International Journal of Molecular Sciences* 19(10).
- Asakawa M, Fukutani Y, Savangsuksa A, Noguchi K, Matsunami H, Yohda M. (2017) Modification of the response of olfactory receptors to acetophenone by CYP1a2. *Sci Rep.* 7(1):10167.
- Barker, P. A. (2004) p75NTR is positively promiscuous: novel partners and new insights. *Neuron.* 42(4): 529-33.
- Bergman U, Ostergren A, Gustafson AL, Brittebo B (2002) Differential effects of olfactory toxicants on olfactory regeneration. *Arch Toxicol.* 76(2):104-12.
- Calof AL, Hagiwara N, Holcomb JD, Mumm JS, Shou J (1996) Neurogenesis and cell death in olfactory epithelium. *J Neurobiol* 30(1):67-81.
- Carr VM, Farbman AI, Colletti LM, Morgan JI (1991) Identification of a new non-neuronal cell type in rat olfactory epithelium. *Neuroscience* 45:433-49.
- Carter LA, Roskams AJ (2002) Neurotrophins and their receptors in the primary olfactory neuraxis. *Microsc Res Tech* 58(3):189-96.
- Chakraborty S, Castranova V, Perez MK, Piedimonte G (2017) Nanoparticles-induced apoptosis of human airway epithelium is mediated by proNGF/p75NTR signaling. *J Toxicol Environ Health A* 80(1):53-68.

- Challis RC, Tian H, Wang J, He J, Jiang J, Chen X, Yin W, Connelly T, Ma L, Yu CR, Pluznick JL, Storm DR, Huang L, Zhao K, Ma M (2015) An Olfactory Cilia Pattern in the Mammalian Nose Ensures High Sensitivity to Odors. *Curr Biol* 25(19):2503-12.
- Clapp TR, Medler KF, Damak S, Margolskee RF, & Kinnamon SC (2006) Mouse taste cells with G protein-coupled taste receptors lack voltage-gated calcium channels and SNAP-25. *BMC Biology* 4, 1–9.
- Coppola DM, Waggener CT, Radwani SM, Brooks DA (2013) An electroolfactogram study of odor response patterns from the mouse olfactory epithelium with reference to receptor zones and odor sorptiveness. *J Neurophysiol* 109(8):2179-91.
- Coppola DM, Ritchie BE, Craven BA (2017) Tests of the sorption and olfactory "fovea" hypotheses in the mouse. *J Neurophysiol* 118(5):2770-2788.
- Costanzo RM, Graziadei PP (1983) A quantitative analysis of changes in the olfactory epithelium following bulbectomy in hamster. *J Comp Neurol* 215(4):370-81.
- Ding X, Dahl AR (2003) Olfactory mucosa: composition, enzymatic localization, metabolism. In: *Handbook of Olfaction and Gustation*, 2nd ed, (Doty RL, ed). pp. 51–73. New York: Marcel Dekker.
- Doty RL, Kamath V (2014) The influences of age on olfaction: a review. *Front Psychol* 5:20.
- Doyle, KL, Cunha C, Hort Y, Tasan R, Sperk G, Shine J, & Herzog H (2018) Role of neuropeptide Y (NPY) in the differentiation of Trpm-5-positive olfactory microvillar cells. *Neuropeptides* 68(March), 90–98.
- Dunston D, Ashby S, Krosnowski K, Ogura T, & Lin W (2013) An Effective Manual Deboning Method To Prepare Intact Mouse Nasal Tissue With Preserved Anatomical Organization. *Journal of Visualized Experiments* (78) 1–7.
- Elsaesser R, Montani G, Tirindelli R, & Paysan J (2005) Phosphatidyl-inositide signalling proteins in a novel class of sensory cells in the mammalian olfactory epithelium. *European Journal of Neuroscience* 21(10), 2692–2700.
- Ferreira T, Miura K, Chef B, Eglinger J (2016) Scripts: BAR.
- Fu Z, Ogura T, Luo W, & Lin W (2018) ATP and Odor Mixture Activate TRPM5-Expressing Microvillous Cells and Potentially Induce Acetylcholine Release to Enhance Supporting Cell Endocytosis in Mouse Main Olfactory Epithelium. *Frontiers in Cellular Neuroscience* 12:71.
- Gaafar H, Girgis R, Hussein M, el-Nemr F (1992) The effect of ammonia on the respiratory nasal mucosa of mice. A histological and histochemical study. *Acta Otolaryngol* 112(2):339-42.

- Genovese F, Tizzano M. (2018) Microvillous cells in the olfactory epithelium express elements of the solitary chemosensory cell transduction signaling cascade. *PLoS One* 13(9):e0202754. doi: 10.1371/journal.pone.0202754.
- Gerbe F, Sidot E, Smyth DJ, Ohmoto M, Matsumoto I, Dardalhon V, Cesses P, Garnier L, Pouzolles M, Brulin B, Bruschi M, Harcus Y, Zimmermann VS, Taylor N, Maizels RM, Jay P (2016) Intestinal epithelial tuft cells initiate type 2 mucosal immunity to helminth parasites. *Nature*. 529(7585):226-30.
- Gerdes J, Schwab U, Lemke H, Stein H (1983) Production of a mouse monoclonal antibody reactive with a human nuclear antigen associated with cell proliferation. *Int J Cancer* 15;31(1):13-20.
- Gokoffski KK, Kawauchi S, Wu HH, Santos R, Hollenbeck PLW, Lander AD, Calof AL (2010) Feedback Regulation of Neurogenesis in the Mammalian Olfactory Epithelium: New Insights from Genetics and Systems Biology. Boca Raton (FL): CRC Press/Taylor & Francis. In: *The Neurobiology of Olfaction*. Chapter 10. *Frontiers in Neuroscience*. Menini A, editor.
- Graziadei GA, Graziadei PP (1979) Neurogenesis and neuron regeneration in the olfactory system of mammals. II. Degeneration and reconstitution of the olfactory sensory neurons after axotomy. *J Neurocytol* 8(2):197-213.
- Gussing F, Bohm S (2004) NQO1 activity in the main and the accessory olfactory systems correlates with the zonal topography of projection maps. *Eur J Neurosci* 19(9):2511-8.
- Hansen A & Finger TE (2008) Is TrpM5 a reliable marker for chemosensory cells? Multiple types of microvillous cells in the main olfactory epithelium of mice. *BMC Neuroscience* 9(1), 115.
- Hardisty JF, Garman RH, Harkema JR, Lomax LG, Morgan KT (1999) Histopathology of nasal olfactory mucosa from selected inhalation toxicity studies conducted with volatile chemicals. *Toxicol Pathol*; 27:618-27.
- Hazardous Substances Data Bank [Internet]. Bethesda (MD): National Library of Medicine (US); Hazardous Substances Databank Number (s): 1336-21-6, 141-78-6, 121-44-8, 79-09-4. (NLM HSDB). <http://toxnet.nlm.nih.gov/cgi-bin/sis/htmlgen?HSDB>
- Hegg CC, Jia C, Chick WS, Restrepo D, Hansen A (2010) Microvillous cells expressing IP3 receptor type 3 in the olfactory epithelium of mice. *Eur J Neurosci* 32(10):1632-45.
- Heydel JM, Menetrier F, Belloir C, Canon F, Faure P, Lirussi F, Chavanne E, Saliou JM, Artur Y, Canivenc-Lavier MC, Briand L, Neiers F (2019) Characterization of rat glutathione transferases in olfactory epithelium and mucus. *PLoS One* 14(7):e0220259.

- Howitt MR, Lavoie S, Michaud M, Blum AM, Tran SV, Weinstock JV, Gallini CA, Redding K, Margolskee RF, Osborne LC, Artis D, Garrett WS (2016) Tuft cells, taste-chemosensory cells, orchestrate parasite type 2 immunity in the gut. *Science* 351(6279):1329-33.
- Huard JM, Youngentob SL, Goldstein BJ, Luskin MB, Schwob JE (1998) Adult olfactory epithelium contains multipotent progenitors that give rise to neurons and non-neural cells. *J Comp Neurol*. 400(4):469-86.
- Iwai N, Zhou Z, Roop DR, Behringer RR (2008) Horizontal basal cells are multipotent progenitors in normal and injured adult olfactory epithelium. *Stem Cells* 26:1298-306.
- Jacquot L, Pourie G, Buron G, Monnin J, Brand G (2006) Effects of toluene inhalation exposure on olfactory functioning: Behavioral and histological assessment. *Toxicology Letters* 165(1): 57–65.
- Jia C, Hayoz S, Hutch CR, Iqbal TR, Pooley AE, Hegg CC (2013) An IP3R3- and NPY-Expressing Microvillous Cell Mediates Tissue Homeostasis and Regeneration in the Mouse Olfactory Epithelium. *PLoS ONE* 8(3).
- Jia C, Hegg CC (2015) Effect of IP3R3 and NPY on age-related declines in olfactory stem cell proliferation. *Neurobiol Aging* 36(2):1045-56.
- Jia C, Sangsiri S, Belock B, Iqbal TR, Pestka JJ, Hegg CC (2011) ATP Mediates Neuroprotective and Neuroproliferative Effects in Mouse Olfactory Epithelium following Exposure to Satratoxin G In Vitro and In Vivo. *Toxicol Sci* 124(1): 169–178.
- Joiner AM, Green WW, McIntyre JC, Allen BL, Schwob JE, Martens JR (2015) Primary Cilia on Horizontal Basal Cells Regulate Regeneration of the Olfactory Epithelium. *J Neurosci* 35(40):13761-72.
- Kapur JN, Sahoo PK, Wong AKC (1985) A new method for gray-level picture thresholding using the entropy of the histogram. *Computer Vision, Graphics, and Image Processing* 29(3): 273-285.
- Kim J, Choi Y, Ahn M, Ekanayake P, Tanaka A, Matsuda H, Shin T (2019) Microglial and astroglial reaction in the olfactory bulb of mice after Triton X-100 application. *Acta Histochem*. 121(5):546-552. doi: 10.1016/j.acthis.2019.04.003.
- Kim JW, Hong SL, Lee CH, Jeon EH, Choi AR (2010) Relationship between olfactory function and olfactory neuronal population in C57BL6 mice injected intraperitoneally with 3-methylindole. *Otolaryngology–Head and Neck Surgery* 143(6): 837–842.
- Kimbell JS, Godo MN, Gross EA, Joyner DR, Richardson RB, Morgan KT (1997) Computer simulation of inspiratory airflow in all regions of the F344 rat nasal passages. *Toxicol Appl Pharmacol* 145(2):388-98.

- Kudo H, Doi Y, Fujimoto S (2010) Expressions of the multidrug resistance-related proteins in the rat olfactory epithelium: a possible role in the phase III xenobiotic metabolizing function. *Neurosci Lett.* 468(2):98-101.
- Kwon BS, Kim MK, Kim WH, Pyo JS, Cheon YH, Cha CI, Nam SY, Baik TK, Lee BL (2005) Age-related changes in microvillar cells of rat olfactory epithelium. *Neurosci Lett.* 378(2):65-9.
- Lemons K, Fu Z, Aoudé I, Ogura T, Sun J, Chang J, Mbonu K, Matsumoto I, Arakawa H, Lin W (2017) Lack of TRPM5-Expressing Microvillous Cells in Mouse Main Olfactory Epithelium Leads to Impaired Odor-Evoked Responses and Olfactory-Guided Behavior in a Challenging Chemical Environment. *Eneuro* 4(3) ENEURO.0135-17.2017.
- Leung CT, Coulombe PA, Reed RR (2007) Contribution of olfactory neural stem cells to tissue maintenance and regeneration. *Nature Neuroscience* 10(6): 720–726.
- Lin W, Margolskee R, Donnert G, Hell SW, Restrepo D (2007) Olfactory neurons expressing transient receptor potential channel M5 (TRPM5) are involved in sensing semiochemicals. *Proc Natl Acad Sci U S A* 104(7):2471-6.
- Lin W, Ezekwe EA Jr, Zhao Z, Liman ER, Restrepo D (2008) TRPM5-expressing microvillous cells in the main olfactory epithelium. *BMC Neuroscience*, 9: 114.
- Loo AT, Youngentob SL, Kent PF, Schwob JE (1996) The aging olfactory epithelium: neurogenesis, response to damage, and odorant-induced activity. *Int J Dev Neurosci.* 14(7-8):881-900.
- Matsumoto I, Ohmoto M, Narukawa M, Yoshihara Y, Abe K (2011) Skn-1a (Pou2f3) specifies taste receptor cell lineage. *Nat Neurosci* 14(6):685-7.
- Meeker R, Williams K. Dynamic nature of the p75 neurotrophin receptor in response to injury and disease (2014) *J Neuroimmune Pharmacol* 9, (5), 615-28.
- Miller ML, Andringa A, Evans JE, Hastings L (1995) Microvillar cells of the olfactory epithelium: morphology and regeneration following exposure to toxic compounds. *Brain Research* 669(1): 1–9.
- Miyawaki A, Homma H, Tamura H, Matsui M, Mikoshiba K (1996). Zonal distribution of sulfotransferase for phenol in olfactory sustentacular cells. *EMBO J* 15(9):2050-5.
- Montani G, Tonelli S, Elsaesser R, Paysan J, Tirindelli R (2006) Neuropeptide Y in the olfactory microvillar cells. *European Journal of Neuroscience* 24(1): 20–24.
- Moran DT, Rowley JC 3rd, Jafek BW (1982) Electron microscopy of human olfactory epithelium reveals a new cell type: the microvillar cell. *Brain Res* 253(1-2):39-46.



- Nagashima A, Touhara K. (2010) Enzymatic conversion of odorants in nasal mucus affects olfactory glomerular activation patterns and odor perception. J Neurosci. 30(48):16391-8.
- Ogura T (2002) Acetylcholine increases intracellular  $\text{Ca}^{2+}$  in taste cells via activation of muscarinic receptors. J Neurophysiol. 87(6):2643-9.
- Ogura T, Krosnowski K, Zhang L, Bekkerman M, Lin W (2010) Chemoreception Regulates Chemical Access to Mouse Vomeronasal Organ: Role of Solitary Chemosensory Cells. PLoS One. 5(7): e11924.
- Ogura T, Szebenyi S, Krosnowski K, Sathyanesan A, Jackson J, Lin W (2011) Cholinergic microvillous cells in the mouse main olfactory epithelium and effect of acetylcholine on olfactory sensory neurons and supporting cells. Journal of Neurophysiology 106(3): 1274–1287.
- Otsu, N (1979) A threshold selection method from gray-level histograms. IEEE Trans. Sys., Man., Cyber. 9: 62-66.
- Pfister S, Dietrich MG, Sidler C, Fritschy JM, Knuesel I, Elsaesser R (2012) Characterization and turnover of CD73/IP3R3-positive microvillar cells in the adult mouse olfactory epithelium. Chemical Senses 37(9): 859–868.
- Pfister S, Weber T, Härtig W, Schwerdel C, Elsaesser R, Knuesel I, Fritschy JM (2015) Novel role of cystic fibrosis transmembrane conductance regulator in maintaining adult mouse olfactory neuronal homeostasis. J Comp Neurol 523(3):406-30.
- Pozharskaya T, Liang J, Lane AP (2013) Regulation of inflammation-associated olfactory neuronal death and regeneration by the type II tumor necrosis factor receptor. Int Forum Allergy Rhinol. (9):740-7.
- Preibisch S, Saalfeld S, Tomancak P (2009) Globally optimal stitching of tiled 3D microscopic image acquisitions. Bioinformatics 25(11):1463-1465.
- Reese TA, Liang H, Tager AM, Luster AD, Rooijen N. Van, Voehringer D, Locksley RM (2007) Chitin induces accumulation in tissue of innate immune cells associated with allergy. Nature 447(7140): 92-6.
- Reisert J, Bauer PJ, Yau KW, Frings S (2003) The Ca-activated  $\text{Cl}^-$  channel and its control in rat olfactory receptor neurons. J Gen Physiol. 122(3):349-63.
- Ressler KJ, Sullivan SL, Buck LB (1993) A zonal organization of odorant receptor gene expression in the olfactory epithelium. Cell 73:597-609.
- Sathyanesan A, Ogura T, Lin W (2012) Automated measurement of nerve fiber density using line intensity scan analysis. J Neurosci Methods 206:165-75.

- Sathyanesan, Aaron. (2017). ImageJ Line scan analysis - Including Hessian feature detection for image stacks.  
[https://www.researchgate.net/publication/312593741\\_ImageJ\\_Line\\_scan\\_analysis\\_-\\_Including\\_Hessian\\_feature\\_detection\\_for\\_image\\_stacks](https://www.researchgate.net/publication/312593741_ImageJ_Line_scan_analysis_-_Including_Hessian_feature_detection_for_image_stacks)
- Saunders CJ, Reynolds SD, Finger, TE (2013) Chemosensory Brush Cells of the Trachea. A Stable Population in a Dynamic Epithelium. *Am J Respir Cell Mol Biol.* 49(2): 190–196.
- Schneider C, O'Leary CE, von Moltke J, Liang HE, Ang QY, Turnbaugh PJ, Radhakrishnan S, Pellizzon M, Ma A, Locksley RM (2018) A Metabolite-Triggered Tuft Cell-ILC2 Circuit Drives Small Intestinal Remodeling. *Cell* 174(2):271-284.
- Schoenfeld TA, Cleland TA (2005) The anatomical logic of smell. *Trends Neurosci* 28(11):620-7.
- Schoenfeld TA, Cleland TA (2006) Anatomical contributions to odorant sampling and representation in rodents: zoning in on sniffing behavior. *Chem Senses* 31(2):131-44.
- Scholzen T, Gerdes J (2000) The Ki-67 protein: from the known and the unknown. *J Cell Physiol* 182(3):311-22.
- Schwob JE, Jang W, Holbrook EH, Lin B, Herrick DB, Peterson JN, Hewitt Coleman J (2017) Stem and progenitor cells of the mammalian olfactory epithelium: Taking poietic license. *J Comp Neurol* 525(4):1034-1054.
- Scott JW (2006) Sniffing and spatiotemporal coding in olfaction. *Chem Senses* 31(2):119-30.
- Scott JW, Sherrill L, Jiang J, Zhao K (2014) Tuning to odor solubility and sorption pattern in olfactory epithelial responses. *J Neurosci* 34(6):2025-36.
- Simpson PJ, Wang E, Moon C, Matarazzo V, Cohen DR, Liebl DJ, Ronnett GV (2003). Neurotrophin-3 signaling maintains maturational homeostasis between neuronal populations in the olfactory epithelium. *Mol Cell Neurosci* 24(4):858-74.
- Stephan AB, Tobochnik S, Dibattista M, Wall CM, Reisert J, Zhao H (2011) The Na(+)/Ca(2+) exchanger NCKX4 governs termination and adaptation of the mammalian olfactory response. *Nat Neurosci.* 15(1):131-7.
- Suzuki Y, Takeda M, Farbman AI (1996) Supporting cells as phagocytes in the olfactory epithelium after bulbectomy. *J Comp Neurol* 376: 509-17.
- Szebenyi S, Ogura T, Sathyanesan A, AlMatrouk A, Chang J, Lin W (2014) Increases in intracellular calcium via activation of potentially multiple phospholipase C isozymes in mouse olfactory neurons. *Front Cell Neurosci.* 8: 336.

- Thiebaud N, Menetrier F, Belloir C, Minn AL, Neiers F, Artur Y, Le Bon AM, Heydel JM (2011) Expression and differential localization of xenobiotic transporters in the rat olfactory neuro-epithelium. *Neurosci Lett* 505(2):180-5.
- Thiebaud N, Veloso Da Silva S, Jakob I, Sicard G, Chevalier J, Ménétrier F, Berdeaux O, Artur Y, Heydel JM, Le Bon AM (2013). Odorant metabolism catalyzed by olfactory mucosal enzymes influences peripheral olfactory responses in rats. *PLoS One* 8(3):e59547.
- Ueha R, Ueha S, Kondo K, Sakamoto T, Kikuta S, Kanaya K, Nishijima H, Matsushima K, Yamasoba T (2016a) Damage to Olfactory Progenitor Cells Is Involved in Cigarette Smoke-Induced Olfactory Dysfunction in Mice. *Am J Pathol.* (3):579-86. doi: 10.1016/j.ajpath.2015.11.009.
- Ueha R, Ueha S, Sakamoto T, Kanaya K, Suzukawa K, Nishijima H, Kikuta S, Kondo K, Matsushima K, Yamasoba T (2016b) Cigarette Smoke Delays Regeneration of the Olfactory Epithelium in Mice. *Neurotox Res.* (2):213-24. doi: 10.1007/s12640-016-9617-5.
- Ueha R, Shichino S, Ueha S, Kondo K, Kikuta S, Nishijima H, Matsushima K, Yamasoba T (2018) Reduction of Proliferating Olfactory Cells and Low Expression of Extracellular Matrix Genes Are Hallmarks of the Aged Olfactory Mucosa. *Front Aging Neurosci* 10:86.
- Vassar R, Ngai J, Axel R (1993) Spatial segregation of odorant receptor expression in the mammalian olfactory epithelium. *Cell* 74:309-18.
- Vedin V, Molander M, Bohm S, Berghard A (2009) Regional differences in olfactory epithelial homeostasis in the adult mouse. *Journal of Comparative Neurology* 513(4): 375–384.
- von Moltke J, Ji M, Liang HE, Locksley RM (2016) Tuft-cell-derived IL-25 regulates an intestinal ILC2-epithelial response circuit. *Nature* 529(7585):221-5.
- Weng PL, Vinjamuri M, Ovitt CE (2016) Ascl3 transcription factor marks a distinct progenitor lineage for non-neuronal support cells in the olfactory epithelium. *Sci Rep* 6:38199.
- Whitby-Logan GK, Weech M, Walters E (2004). Zonal expression and activity of glutathione S-transferase enzymes in the mouse olfactory mucosa. *Brain Res* 995(2):151-7.
- Xie F, Fang C, Schnittke N, Schwob JE, Ding X (2013) Mechanisms of permanent loss of olfactory receptor neurons induced by the herbicide 2,6-dichlorobenzonitrile: effects on stem cells and noninvolvement of acute induction of the inflammatory cytokine IL-6. *Toxicol Appl Pharmacol.* 272(3):598-607. doi: 10.1016/j.taap.2013.07.020. Epub 2013 Aug 4.
- Yamaguchi T, Yamashita J, Ohmoto M, Aoudé I, Ogura T, Luo W, Bachmanov AA, Lin W, Matsumoto I, Hirota, J (2014) Skn-1a/Pou2f3 is required for the generation of Trpm5-

- expressing microvillous cells in the mouse main olfactory epithelium. BMC Neuroscience 15:13.
- Yen JC, Chang FJ, Chang S (1995) A new criterion for automatic multilevel thresholding. IEEE Trans Image Process. 4(3):370-8.
- Yoshihara Y, Kawasaki M, Tamada A, Fujita H, Hayashi H, Kagamiyama H, Mori K (1997) OCAM: A new member of the neural cell adhesion molecule family related to zone-to-zone projection of olfactory and vomeronasal axons. J Neurosci 17(15):5830-42.
- Zhang X, Rogers M, Tian H, Zhang X, Zou DJ, Liu J, Ma M, Shepherd GM, Firestein SJ (2004) High-throughput microarray detection of olfactory receptor gene expression in the mouse. Proc Natl Acad Sci U S A. 101(39):14168-73.
- Zufall F, Firestein S, Shepherd GM (1991) Analysis of single cyclic nucleotide-gated channels in olfactory receptor cells. J Neurosci. 11(11):3573-80.